CSIC - Universidad de Salamanca
Instituto de Biología Molecular y Celular del Cáncer
Centro de Investigación del Cáncer

CHARACTERIZATION OF NEW REGULATORY MECHANISMS AND METABOLIC ROLES FOR VAV PROTEINS

Ph.D. THESIS

SONIA RODRÍGUEZ FERNÁNDEZ

SALAMANCA, JULY 2019

CENTRO DE INVESTIGACIÓN DEL CÁNCER

Universidad de Salamanca-CSIC
CSIC

Campus Miguel de Unamuno
37007 Salamanca, España
Tel. +34 923 29 47 20
Fax +34 923 29 47 43
www.cicancer.org

El **Dr. XOSÉ RAMÓN GARCÍA BUSTELO**, Profesor de Investigación del Consejo Superior de Investigaciones Científicas en el Centro de Investigación del Cáncer de Salamanca y el Instituto de Biología Molecular y Celular del Cáncer de Salamanca,

CERTIFICA:

Que el trabajo de tesis titulado **"Characterization of new regulatory mechanisms and metabolic roles for Vav proteins"**, presentado por **Dña. SONIA RODRÍGUEZ FERNÁNDEZ** para optar al grado de Doctor en Biología por la Universidad de Salamanca, ha sido realizado bajo mi dirección en el Centro de Investigación del Cáncer. Considerando que cumple con las condiciones necesarias, autorizo su presentación a fin que pueda ser defendido ante el tribunal correspondiente.

Y para que conste a los efectos oportunos, expido y firmo el presente certificado en Salamanca, a 5 de junio de 2019.

Fdo. Dr. Xosé Ramón García Bustelo

ABSTRACT

Vav proteins are signal transductors that play bivalent roles as Rho GTPase nucleotide exchange factors and adaptor proteins. In mammals, the family is composed of three members (Vav1, Vav2 and Vav3) that share a distinctive and highly conserved domain structure. These proteins play overlapping but not redundant roles in a wide range of physiological and pathological processes. It is also well known that their regulation is tightly controlled by tyrosine phosphorylation–dependent conformational changes. However, information about other regulatory layers or the contribution of catalytic and adaptor activities to organismal physiology is still lacking. Our findings had led to the identification and characterization of two novel phosphoinositide– and lysine acetylation–mediated regulatory mechanisms for Vav1 in T cells. In addition, we have unveiled a new catalysis–dependent role of Vav2 in IGF-1 and insulin signaling in skeletal muscle. Altogether, these data expand the current knowledge of Vav proteins in terms of family member– and tissue–specific activation processes. They also shed light into previously unknown functions of Vav2 in skeletal muscle biology and metabolic homeostasis.

FINANTIAL SUPPORT

This work has been supported by grants from the Castilla–León Government (CSI252P18, CLC–2017–01), the Spanish Ministry of Science, Innovation and Universities (MSIU) (SAF2015–64556–R), Worldwide Cancer Research (14–1248), the Ramón Areces Foundation, and the Spanish Association against Cancer (GC16173472GARC).

Our institution is supported by the Programa de Apoyo a Planes Estratégicos de Investigación de Estructuras de Investigación de Excelencia of the Castilla–León autonomous government (CLC–2017–01).

My graduate student contract has been mostly supported by the MSIU (BES–2013–063573) and currently by funding linked to the CLC–2017–01 grant.

Both Spanish and Castilla–León government–associated funding is partially supported by the European Regional Development Fund.

TABLE OF CONTENTS

FIGURE INDEX

TABLE INDEX

LIST OF ABBREVIATIONS

4EBP1	4E binding protein-1
Ac	Acidic
AS160	Akt substrate of 160 kDa
BAT	Brown adipose tissue
BCR	B cell receptor
bFGF	Basic fibroblast growth factor
CCK	Cholecystokinin
CD	Chow diet
CH	Calponin homology
CSH3	C–terminal SH3 domain of Vav proteins
DAG	Diacylglycerol
DH	Dbl–homology domain
EE	Energy expenditure
EGF	Epidermal growth factor
EGFP	Enhanced green fluorescent protein
ERK	Extracellular signal–regulated kinase
FGF21	Fibroblast growth factor 21
FOXO1	Forkhead box protein O1
FOXO3	Forkhead box protein O3
GAP	GTPase–activating protein
GDI	Guanine nucleotide dissociation inhibitor
GDP	Guanosine diphosphate
GEF	Guanosine nucleotide exchange factor
GLP-1	Glucagon–like peptide 1
GS	Glycogen synthase
GSK3	Glycogen synthase kinase 3
GTP	Guanosine triphosphate
GTPase	Guanosine triphosphatase
HFD	High fat diet
IGF-1	Insulin–like growth factor 1
Il-15	Interleukin 15
Il-6	Interleukin 6
IR	Insulin receptor
IRS	Insulin receptor substrate
JNK	C–Jun N–terminal kinase
KR	Lysine rich region
KR1	N–part of the KR
KR2	C–part of the KR
LIF	Leukemia inhibitory factor
LPA	Lysophosphatidic acid
LPC	Lysophosphatidylcholine
MEK1/2	Mitogen–activated protein kinase/extracellular signal–regulated kinase kinase 1/2
MHC	Myosin heavy chain
mTORC1	Mammalian target of rapamycin complex 1
mTORC2	Mammalian target of rapamycin complex 2
NFAT	Nuclear factor of activated T-cells
NRG4	Neuregulin 4
NSH3	N–terminal SH3 domain of Vav proteins
PA	Lysophosphatidic acid
PC	Phosphatidylcholine
PDK1	Pyruvate dehydrogenase kinase 1
PE	Phosphatidylethanolamine
PEPCK	Phosphoenolpyruvate carboxykinase
PH	Plekstrin-homology domain
PI(3,4)P_2	Phosphatidylinositol (3,4)-bisphosphate
PI(3,5)P_2	Phosphatidylinositol (3,5)-bisphosphate
PI(4,5)P_2	Phosphatidylinositol (4,5)-bisphosphate
PI3K	Phosphatidylinositol-3 kinase
PI3P	Phosphatidylinositol-3-phosphate
PI4P	Phosphatidylinositol-4-phosphate
PI5P	Phosphatidylinositol-5-phosphate
PIP2	Phosphatidylinositol (4,5)-bisphosphate
PIP3	Phosphatidylinositol (3,4,5)-triphosphate
PLCγ	Phospholipase C gamma
PRR	Proline-rich region
PS	Phosphatidylserine
PTK	Protein tyrosine kinase
PYY	Peptide YY
RQ	Respiratory quotient
S1P	Sphingosine 1-phosphate
S6K	p70 ribosomal protein S6 kinase
SH2	Src homology 2
SH3	Src homology 3
SNP	Single nucleotide polymorphism
SRF	Serum response factor
TCR	T cell receptor
TNFα	Tumor necrosis factor alpha
TSC2	Tuberin
VCO_2	Volume of CO_2
VO_2	Volume of O_2
WAT	White adipose tissue
ZF	Zinc finger

INTRODUCTION

1. VAV FAMILY

Vav proteins play bivalent roles as GDP/GTP exchange factors for Rho GTPases and as signaling adaptors downstream of protein tyrosine kinases. The family originated in choanozoans, the closest unicellular relatives of metazoans, and expanded in vertebrates to the three members composition found in mammals. The biological functions of Vav proteins are tightly regulated by tyrosine phosphorylation and they play important roles in different tissues, including the immune, the cardiovascular or the nervous system. Aside from their developmental and effector functions in these cell lineages, Vav proteins have also been linked to tumorigenic processes.

1.1. Canonical role as Rho guanosine nucleotide exchange factors

Rho guanosine triphosphatases (GTPases) are a family of small proteins that act as molecular switches. They are involved in a wide range of physiological and pathological processes [1]. Although mainly known for their essential role in the regulation of actin cytoskeleton, Rho GTPases participate in many other signaling transduction pathways. These include the establishment of cell polarity, microtubule dynamics, transcriptional regulation or vesicular transport [2-7].

This variety of responses requires a tight spatiotemporal regulation that is exerted by different guanosine nucleotide exchange factors (GEFs), GTPase–activating proteins (GAPs) and guanine nucleotide dissociation inhibitors (GDIs). GEFs stimulate the release of the nucleoside guanosine diphosphate (GDP) from the GTPase to allow the binding of guanosine triphosphate (GTP). This promotes the rapid transition of the GTPase from the GDP–bound inactive state to the GTP–bound active form **(Fig. 1)**. GAPs, on the contrary, enhance the intrinsic GTPase activity of Rho proteins favoring the shift from the active to the inactive, GDP-bound state **(Fig. 1)**. Rho GDIs, on the other hand, can sequester the GDP-bound GTPases at the cytosol preventing their activation [8].

There are more than 80 different Rho GEFs in mammals that have evolved to accommodate all the tissue–specific regulatory requirements of Rho GTPases [8]. As the main activators of the GTPases in cells, most GEFs have themselves sophisticated regulatory mechanisms that elicit concrete and cell–specific responses. Consequently, alterations in terms of abundance or gain– and loss–of–function mutations lead to

aberrant Rho GTPase activation and the development of a broad number of physiological alterations and diseases [9, 10].

Vav is probably one of the most studied families of Rho GEFs. Vav proteins activate preferentially members of the Rac subfamily (e.g. Rac1, RhoG), but can also act as GEFs for RhoA subfamily proteins [11, 12]. Their catalysis–dependent pathways are known to be involved in a diversity of biological processes and exert multiple tumorigenic–related functions [12] **(Fig. 1)**.

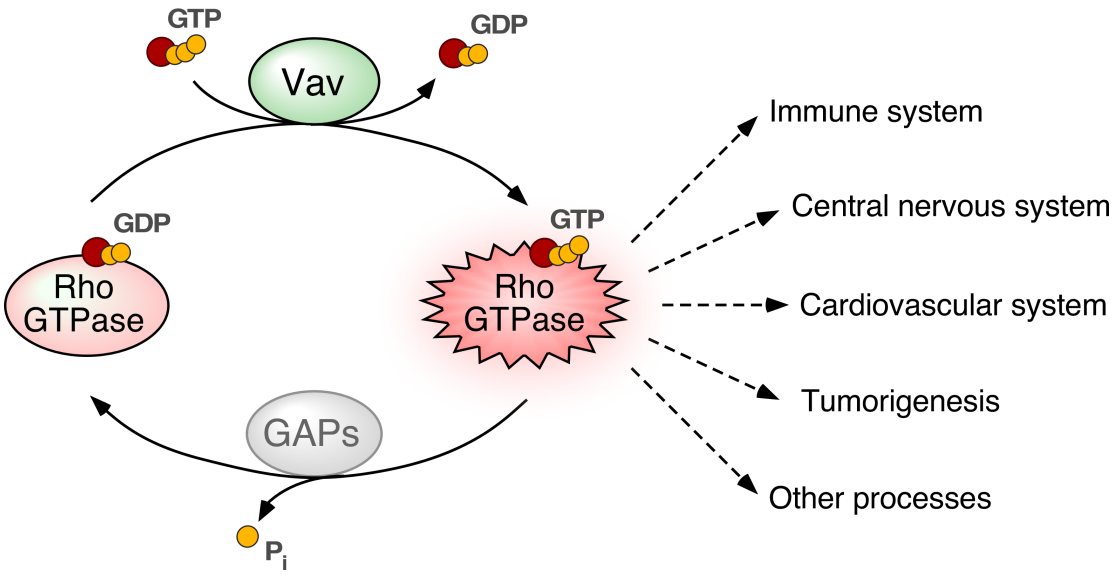

Figure 1. Activation cycle of Rho GTPases and their known Vav-dependent functions. Rho GTPases remain inactive at the cytoplasm in their GDP-bound state and become active upon binding to GTP. GEF proteins, such as Vav, can bind to the switch domain of the GTPases to favor the exchange of GDP for GTP to promote diverse specific responses both at the cellular and organismal level. Hydrolysis of the GTP to GDP stimulated by GAPs returns the Rho protein to the inactive state.

1.2. Phylogenetic evolution

No Vav family members have been found so far in the most basic animal unicellular organisms or in plants. The most primitive family relatives are found in choanozoans, a recently identified group of unicellular organisms considered to be the closest relatives to animal metazoans [13-15]. A single Vav protein is present in invertebrates and urochordates. However, the whole genome duplication events that occurred during the first stages of the evolution of vertebrates led to the common composition of three members (Vav1, Vav2 and Vav3) found in mammals **(Fig. 2)**. The first expansion in the number of family proteins is found in Agnatha, where we can detect a Vav2 analog and a

second family member that shares structural features with the vertebrate Vav1 and Vav3 proteins (referred to here as Vav1/3) **(Fig. 2,** highlighted clade**)**. The three Vav proteins typically found in most vertebrate species are first found in chondrichthyes, probably as a consequence of a gene duplication event that affected the ancestral Vav1/3 gene described above. Interestingly, the origin of Vav1 is associated with the point in evolution in which the adaptive immune system became fully developed [16]. Due to the subsequent genome–duplication process occurred in Teleostei, most bony fishes conserve two *Vav3* genes. Besides, alternative splicing events can yield different protein isoforms in all species [12].

Phylogenetic analyses have also unveiled that, despite the nomenclature, Vav2 is the most ancient protein of the family. Vav1 and Vav3, on the other hand, have emerged later on in evolution from a common ancestor and, accordingly, are more related to each other than to the ancestral Vav2 **(Fig. 2)**.

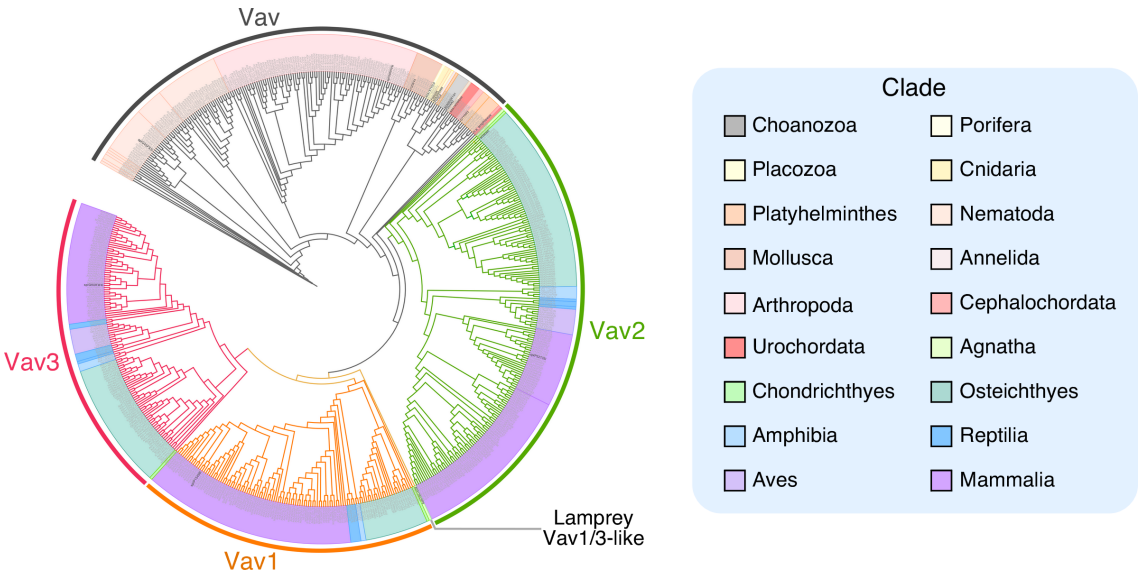

Figure 2. Phylogenetic analysis of the Vav family proteins. Proteins containing DH and SH2 domains were obtained from the UniProt database and the phylogenetic tree reconstructed using the maximum–likelihood method. Node colors indicate if the protein belongs to the single Vav family group (gray color) or the vertebrate Vav1 (orange color), Vav2 (green color) or Vav3 (purple color) branch. The lamprey (*Lethenteron camtschaticum*) Vav1/3–like protein node has been highlighted in light brown. The color code used for each phylogenetic clade is shown on the light blue box (right).

1.3 Structure

Nearly all Vav family proteins contain an evolutionary conserved multidomain structure composed of an N–terminal calponin–homology (CH) domain, an acidic (Ac) region, a

catalytic Dbl–homology (DH) domain, a pleckstrin–homology (PH) region, an atypical C1 subtype zinc finger (ZF) domain, a proline–rich region (PRR), and a SH2 domain that is flankedby a N– (NSH3) and a C–terminal SH3 (CSH3) **(Fig. 3)**. This complex structure is already present in choanozoans and maintained through evolution, with the exception of certain groups of invertebrates in which the PRR and the most N–terminal SH3 (NSH3) have been concurrently or independently lost [17] **(Fig. 4)**.

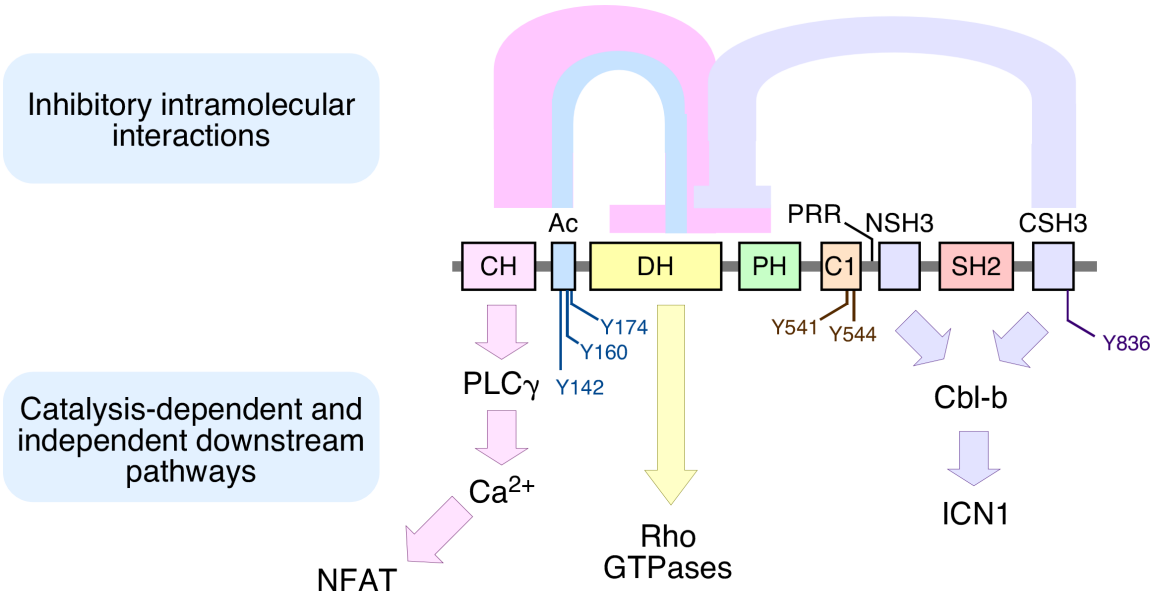

Figure 3. Basic domain structure of vertebrate Vav proteins. The inhibitory intramolecular interactions established between domains are specified with lines at the top. The functions associated to each region and the main regulatory phosphosites (using the primary amino acid sequence corresponding to murine Vav1) are indicated at the bottom.

Remarkably, Vav proteins display two distinctive structural features: a DH-PH-ZF cassette and three consecutive Src homology domains. The former folds together to conform a "catalytic core" involved in the exchange of guanosine. The latter, on the other hand, enable multiple protein–protein interactions [12].

Due to this complex structure, Vav proteins can accomplish both catalytic and non–catalytic functions. Whilst the GEF activity is mediated by the DH in a concerted manner with the adjacent PH and ZF, the adaptor functions are more variegated in terms of effector domains involved and biological outputs achieved. As an example, the Vav1 CH domain is involved in the engagement of a phospholipase C gamma (PLCγ)–dependent pathway that triggers the stimulation of the nuclear factor of activated T cells (NFAT) [12, 18, 19]. On the other hand, the two Vav1 SH3 domains promote a Cbl–b–dependent

tumor suppressor mechanism that promotes the ubiquitinylation–mediated degradation of the active signaling fragment of Notch1 in immature T cells [20] **(Fig. 3**, bottom**).**

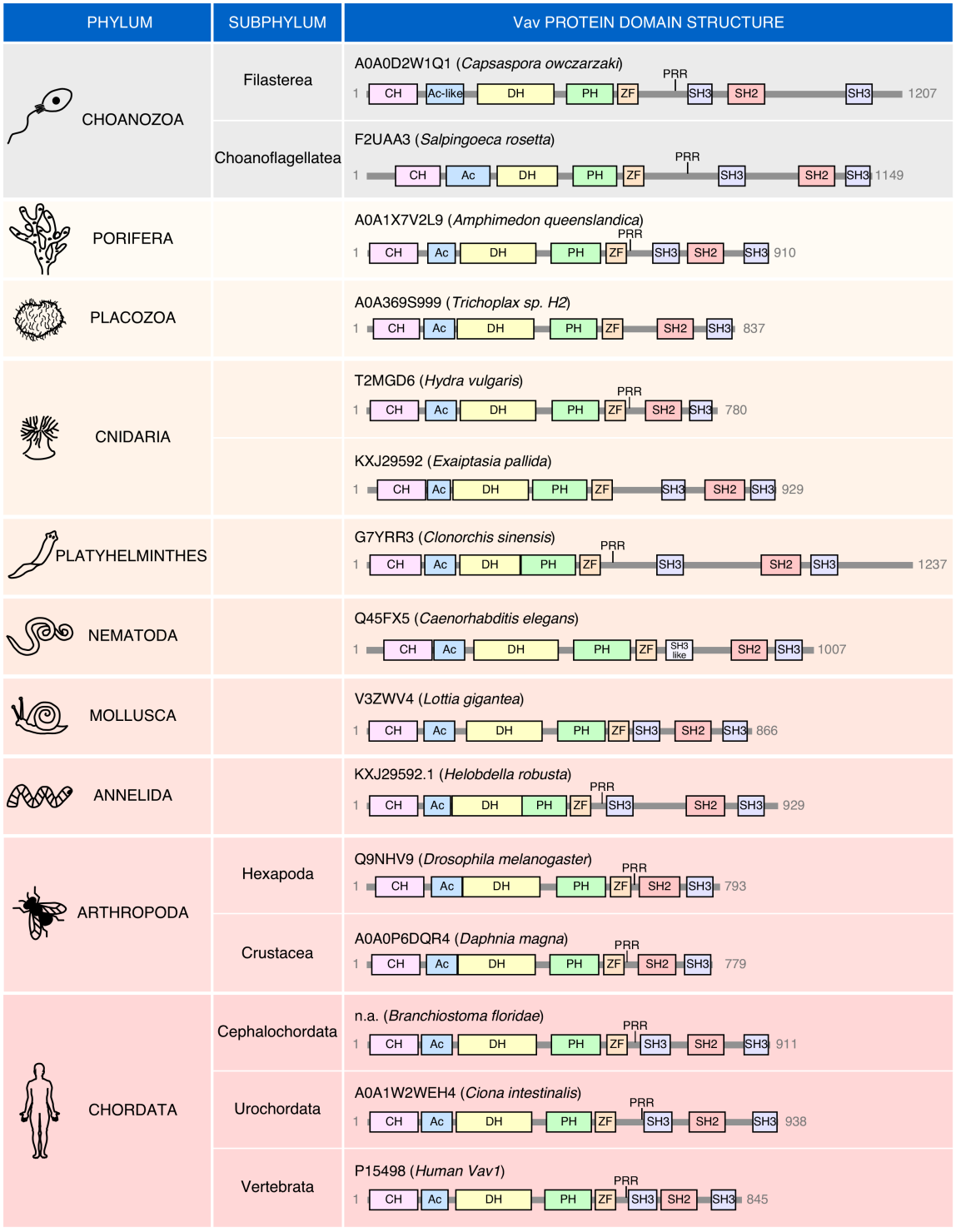

Figure 4. Evolution of the "body plan" of Vav family proteins. Depiction of the structure of Vav proteins in representative organisms of both the Choanozoan (in gray) and Metazoan (salmon color gradient) phyla. UniProt accession codes are indicated for each protein. N.a., not annotated.

The multidomain structure also contributes to the regulation of the biological activity of these proteins. Vav proteins are regulated by a complex intramolecular autoinhibitory mechanism in which the CH, Ac and CSH3 domains intervene. In their inactive state, both ends of the protein are folded over the DH (in the case of the CH and Ac) and the PH (in the case of the CSH3) domains occluding the catalytic site **(Fig. 3)**. This closed conformation inhibits the catalytic and most of the non–catalytic outputs of the proteins [21]. After tyrosine phosphorylation of specific residues, the conformational changes undergone force the release of the inhibitory contacts and the activation of the protein [21-24].

1.4 Regulatory mechanisms

1.4.1 Tyrosine phosphorylation

As indicated above, the biological activity of Vav proteins is mainly controlled by tyrosine phosphorylation–dependent changes in their conformation. This regulatory process is a distinctive characteristic of this family and has been acquired very early on in evolution, since the motifs involved are already present in the choanozoan Vav protein **(Fig. 4).** In addition, functional studies have shown that this regulatory mechanism is conserved at least from *C. elegans* [12, 21, 25, 26].

The nonphosphorylated Vav proteins are inactive due to a "closed" conformation mediated by extensive intramolecular interactions between the CH-Ac and the CSH3 with the catalytic DH-PH-ZF core **(Fig. 3)**. These interdomain interactions occlude the GTPase binding site and, at the same time, favor a conformation of the DH-PH-ZF cassette that is not compatible with full catalytic efficiency [21, 23, 24, 27-29]. Many adaptor–like functions of Vav proteins are also subjected to this type of regulation, indicating that those interdomain interactions also contribute to the occlusion of noncatalytic effector sites of the molecule. By contrast, the suppressor activity of Vav1 that contributes to the buffering of Notch1 signaling can be fully engaged by both the phosphorylated and nonphosphorylated versions of the protein [20]. In stimulated cells, Vav proteins acquire an "open", biologically active state upon becoming phosphorylated on several tyrosine residues located in the Ac (Tyr^{142}, Tyr^{160}, Tyr^{174}), ZF (Tyr^{541}, Tyr^{544}), and CSH3 (Tyr^{836}) domains (please note that the amino acid numbers are given considering those present in the primary sequence of mouse Vav1) [21, 23, 24, 27-30] **(Fig. 3)**. It is not currently known whether the CH-Ac and CSH3 regions fully detach

from the rest of the domains of the molecule during this activation step or whether they remain in contact with other domains using a different spatial orientation. However, functional data obtained using several Vav1 point mutants suggest that the CH-Ac region has to remain bound to other parts of the molecule in order to promote the optimal stimulation of the NFAT pathway in T lymphocytes [31]. In line with this, electron microscopy experiments also suggest that the Vav1 CSH3 maintains interdomain contacts with the catalytic core in the "open" conformation of the protein [21]. It is likely that the foregoing conformational changes are used in additional regulatory steps. For example, the recent use of phosphosite mutant proteins revealed that Vav1 can engage different downstream signaling branches depending on the total number of phosphosites that are phosphorylated at a given time [31]. This suggests that Vav proteins can fluctuate between different conformational and signaling states during cell signaling.

This phosphorylation step is mediated by transmembrane and/or cytosolic protein tyrosine kinases depending on the cell type involved. In the former case, Vav proteins interact directly through its SH2 domain with the autophosphorylated cytoplasmic tails of the tyrosine kinases [32, 33]. However, in the case of cytoplasmic kinases, the process is more complex and involves the interaction of Vav proteins with transmembrane coreceptors or cytosolic adaptor molecules that can be docked onto phosphorylated proteins located at the plasma membrane. These interactions can be SH2-dependent or independent [31, 34-46].

1.4.2 Subcellular localization

Optimal signaling requires an appropriate localization of the protein. This is important not only for their phosphorylation but also for the engagement of downstream effectors. In most cell types analyzed, Vav proteins are mainly found in the cytoplasm and must translocate to the plasma membrane upon stimulation to fulfill their function [22, 27, 46-49].

Several studies have also reported the presence of Vav1 in the nucleus, being its translocation dependent on a nuclear localization signal present in the PH region, the binding of uncharacterized cytoplasmic sequestering factors to the CSH3 and possibly nucleus–specific arginine methylation events [50, 51]. However, the mechanism that elicits this translocation step and subsequent activity of Vav1 in the nucleus remains obscure as yet.

1.4.3 Phosphoinositides

Early studies suggested that diacylglycerol (DAG) and phosphatidylinositol (3,4,5)-trisphosphate (PIP_3) could activate Vav proteins through their interaction with the ZF and the PH domains, respectively [52, 53]. However, such possibility is in conflict with the known inability of those domains to directly bind those second messengers [54-56]. Consistent with this, it has been shown that these Vav domains do not undergo the expected DAG– and PIP_3–dependent changes in subcellular localization when expressed in cells [54, 55]. Later evidences also indicate that Vav proteins act upstream rather than downstream of both PLCγ and phosphoinositide 3–kinase (PI3K) family proteins [57-60], further invalidating those two regulatory models.

1.4.4 Acetylation and other posttranslational modifications

Vav proteins may undergo other posttranslational modifications whose relevance for the activity of these GEFs remains mostly undetermined. Negative regulation of Vav1 by Cbl family proteins–dependent ubiquitination has been proposed by different studies [61-64] and a small nuclear pool of Vav1 has been shown to be arginine–methylated under anti-CD28 stimulation of the T cell antigen receptor (TCR) in T cells [51, 65].

Vav proteins have also been recurrently identified in high throughput acetylome analyses in different cell types [66-70]. However, the role of acetylation, if any, on the regulation of these proteins has not yet been addressed. The study of the functional relevance of this posttranslational modification is one of the goals of this thesis.

1.5 Physiological and pathological roles in mammals

No information is available regarding the role of Vav proteins in non–mammalian vertebrate species. In mammals, most of the genetic evidence regarding the role of Vav proteins has been gathered in mice. Despite sharing the same structure, Vav proteins display overlapping but not redundant functions. They also exhibit different tissular expression patterns. In mammals, Vav1 is primarily detected in hematopoietic cells whereas Vav2 and Vav3 are nearly ubiquitously expressed. They known roles include physiological functions within the immune, the central nervous and the cardiovascular systems as well as in other pathological states such as tumorigenesis [12].

1.5.1. Hematopoiesis

In mammals, the deletion of Vav1 leads to severe defects in lymphocytes. In T cells, Vav1 plays an important role in development, maturation, selection and signaling downstream of the TCR [12, 71-76]. Due to this, Vav1 knockout mice are lymphopenic and defective for several TCR–mediated immune responses [12]. More recent results indicate that Vav1 is also important for the homeostatic production of regulatory T cells [77]. Moreover, the use of knock-in mice expressing Vav1^{R63W}, a natural variant that harbors a CH domain that lacks adaptor functions [78], has revealed that the adaptor functions of this protein can also contribute to the intrathymic negative selection of thymocytes and the production of regulatory T cells [79, 80]. In B cells, however, this protein collaborates in B cell receptor (BCR) signaling and antigen presentation in a non–essential manner [72, 81]. Milder defects have also been observed in other hematopoietic cell types [12]. The other members of the family are also important in the hematopoietic system and reveal a certain grade of redundancy with Vav1 [82]. Vav2 is important for the generation of the peritoneal B_1 cells and the stimulation of optimal humoral immune responses [83]. It also collaborates in T cell responses [84]. Vav3, apart from cooperating with Vav1 and Vav2 in T cell signaling, is important for the normal activity of osteoclasts and the regulation of antifungal innate immunity [82, 85-87].

1.5.2. Central nervous system

Several studies have shown that Vav2 and Vav3 play redundant and non–redundant roles in the nervous system. Both proteins contribute to neurite outgrowth and branching together with axon guidance in early developmental stages [47, 88-90]. Although dispensable for basal dendritic spine formation, both are also needed for spine enlargement in the hippocampus [89, 91]. Vav3 is also involved in a variety of cerebellar functions such as Purkinje cell dendritogenesis, survival and migration of granule cells, and the formation of the cerebellar intercrural fissure during the perinatal period. This leads to motor coordination and gaiting defects in early postnatal periods when Vav3 is genetically inactivated in mice [92]. Vav3 also controls the migration of axons of GABAergic neurons from the caudal to the rostral region of the ventrolateral medulla [93], a brainstem center that controls sympathetic, respiratory, heart, cardiovascular, and renal activities [94]. When Vav3 is absent, this GABAergic wiring is not properly established, leading to the loss of the tonic inhibition exerted by the ventral over the

rostral area of the ventrolateral medulla, and the development of multiple sympathetic-dependent physiological defects in mice [93, 95-97]. Further functions of Vav3 inside the nervous system include the blockage of the differentiation of oligodendrocyte precursors and the promotion of myelination processes during both development and injury recovery [98]. Additional known functions of Vav2 include the negative regulation of the cell surface expression and activity of the dopamine transporter in limbic dopaminergic neuron terminals. An important manifestation of this function is the diminished behavioral response of *Vav2*$^{-/-}$ mice to the administration of cocaine [99].

1.5.3. Cardiovascular system

Mouse models have shown that Vav2 and Vav3 play roles in cardiovascular homeostasis. The depletion of any of these proteins in mouse models leads to a similar phenotype characterized by cardiovascular remodeling, thickening of the aorta walls, hypertension and tachycardia, although the mechanisms involved are different [95, 100]. In the case of *Vav2*$^{-/-}$ mice, the underlying cause are defects in the nitric oxide–mediated relaxation of blood vessels in vascular smooth muscle cells [101, 102]. The depletion of Vav3, however, causes chronic sympathoexcitation due to the loss of inhibitory signals in the ventrolateral medulla that leads, apart from the cardiovascular symptoms, to the development of metabolic syndrome [93, 96, 97].

1.5.4. Other phenotypes

Single nucleotide polymorphisms (SNPs) upregulating *VAV1* expression have been linked to autoimmune encephalomyelitis and multiple sclerosis [103]. Vav2 and Vav3 are also important for the optical nerves, leading its absence to a glaucoma–like phenotype [104]. Genomic studies have also unveiled *VAV2* SNPs associated to total anomalous pulmonary venous connection [105]. *VAV3* SNPs have been linked to schizophrenia, hypothyroidism and susceptibility to candidemia [87, 106-109].

1.5.5. Tumorigenesis

Vav proteins have been linked to tumorigenesis since the moment of their discovery, when an artifactual N–terminal truncated version of Vav1 with transforming properties

was isolated during a focus formation assay used for the identification of novel oncogenes [71].

Due to their role as Rho activators and cytoskeleton regulators, their activity has been associated to cancer cell survival, proliferation, migration, invasion and angiogenesis [12]. Vav1 is ectopically expressed in a subset of neuroblastomas, medulloblastomas, pancreatic duct adenoarcinomas, breast cancer and lung cancer, where it can also be mutated [64, 110-115]. Vav2 and Vav3 are both required for breast tumorigenesis as well as for the initiation and promotion phases of skin tumors [116-118]. High expression of Vav3 is also linked to bad prognosis in prostatic tumors [119, 120]. In the hematopoietic system, Vav1 gain–of–function mutations and translocations have been found in human leukemias and lymphomas [121-124]. Vav1 and Vav3 are important effectors in p190-BCR-ABL–expressing acute lymphoblastic leukemias and Vav1 is also involved in the fitness of c-Kit–driven myeloid leukemias [125-127]. Unexpectedly, it has been recently demonstrated that Vav1 can also exert a tumor suppressor role in TLX+ leukemias [20].

2. METABOLIC REGULATION

The maintenance of energy balance is essential for life. It is determined by the ratio between energy intake (provided by food) and energy expenditure (which depends on basal metabolic rate, adaptive thermogenesis and physical activity) [128]. All the organisms need a systemic regulation of energy able to face alterations in any of those two sides of the scale to preserve metabolic homeostasis. In mammals, such a homeostasis requires the coordinated work of several organs interconnected by endocrine and neural signals **(Fig. 5)**. The feeding behavior and energy expenditure are under the control of the hypothalamus and the brainstem, which integrate the signals received from

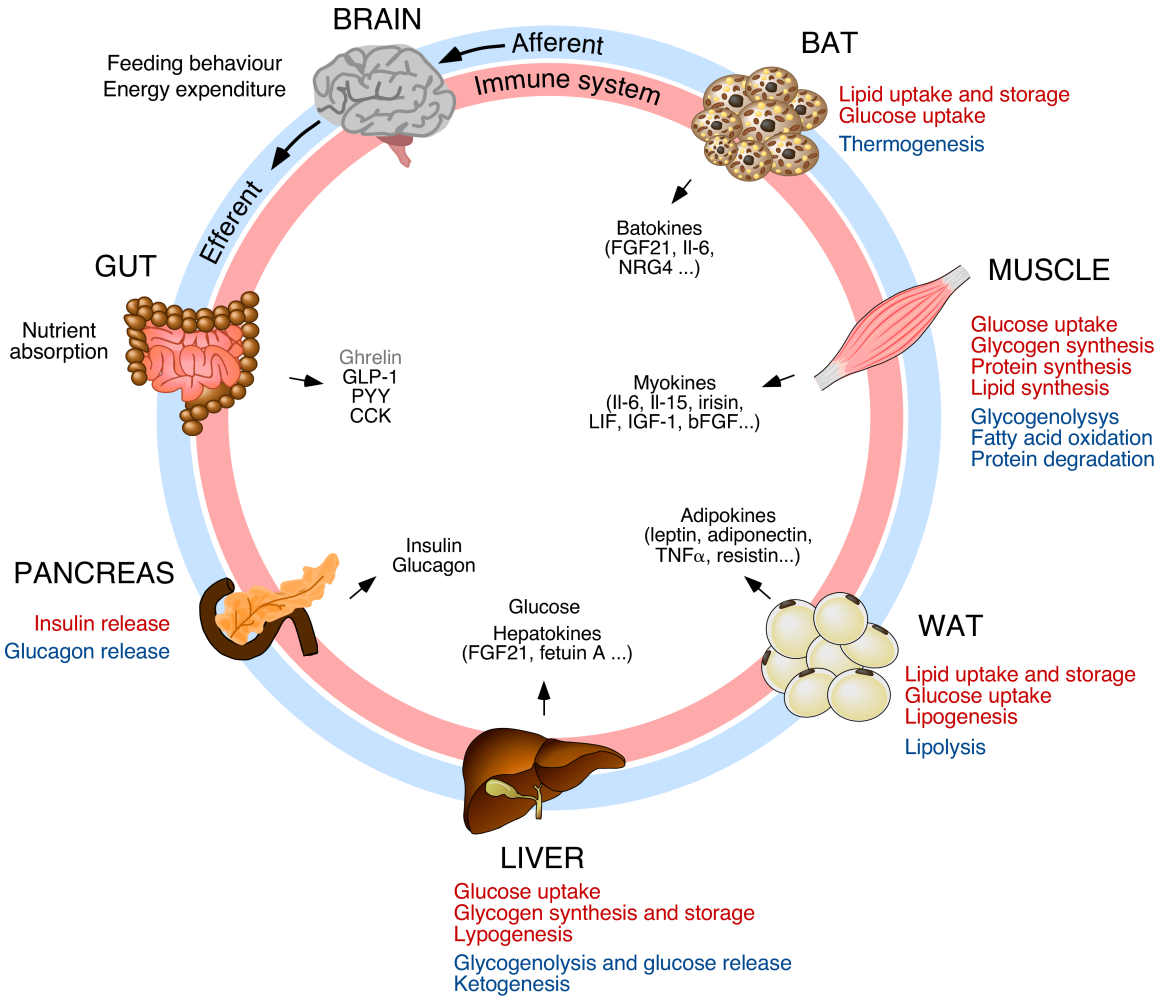

Figure 4. Players involved in metabolic homeostasis. The main anabolic and catabolic pathways occurring in each organ are indicated in red and blue letters respectively. FGF21, fibroblast growth factor 21; Il-6, interleukin 6; NRG4, neuregulin 4; Il-15, interleukin 15; LIF, leukemia inhibitory factor; IGF-1, insulin-like growth factor 1; bFGF, basic fibroblast growth factor; TNFα, tumor necrosis factor alpha; GLP-1, glucagon-like peptide 1; PYY, peptide YY; CCK, cholecystokinin. Anabolic and catabolic pathways are indicated in red and blue, respectively. Modified from *(130)*.

the peripheral tissues and respond via efferent neurons or endocrine signals **(Fig. 5)** [129]. The stomach, digestive tract and the associated microbiota, can also communicate with other organs through the secretion of hormones such as ghrelin, glucose–like peptide 1 and other metabolites **(Fig. 5)** [130]. The pancreas releases insulin or glucagon when blood levels are high or low, respectively. In turn, it can induce different responses in other organs such as the liver, the adipose tissue and the muscle [131] **(Fig. 5)**. Liver is mainly in charge of carbohydrate metabolism and glycogen storage. White and brown adipose tissues (WAT and BAT, respectively) are the main players of lipid metabolism, being their main function fat storage and thermogenesis, respectively [131]. Muscle expends energy through physical activity, accounting for around the 80% of glucose disposal [132]. All these organs can at the same time produce hormone-like substances called hepatokines (in the case of liver), adipokines (in the case of WAT), batokines (in the case of BAT) and myokines (in the case of muscle) that can act in both autocrine and paracrine manner **(Fig. 5)** [133, 134]. On top of that, inflammatory factors and adrenal hormones (glucocorticoids and catecholamines) can also modulate metabolism [135]. Deregulation of any of these processes, causes energy imbalance and the subsequent development of metabolic disorders such as obesity, metabolic syndrome and diabetes [131, 135].

2.1 Insulin signaling and diabetes

Insulin is the main controller of energy homeostasis in the human body. As the main anabolic hormone, dysfunctions in its pathway lead to defects in carbohydrate, lipid and protein metabolism [136]. Independently of the target organ, insulin released from the pancreas is recognized by the insulin receptor (IR). This tyrosine kinase receptor, in turn, phosphorylates the insulin receptor substrate (IRS). IRS triggers the stimulation of PI3K, leading to the production of PIP_3 from phosphatidylinositol-4,5-bisphosphate (PIP_2). Akt, a serine/threonine kinase that modulates cell growth and metabolism, is then recruited to the plasma membrane and activated through phosphorylation. Akt inhibits via phosphorylation the activity of tuberin (TSC2), the forkhead (FoxO) family of transcriptional factors, and glycogen synthase kinase 3 (GSK3). The inhibition of TSC2 unleashes mTOR activity that, in turn, promotes protein synthesis, metabolic programs, and cell growth. The inhibition of FoxO favors the expression of genes involved in cell metabolism, survival, and cycle progression. The inhibition of GSK3 leads to the

stimulation of glycogen synthase (GS) activity, thus favoring the transient storage of glucose as glycogen. Akt also contributes to glucose uptake by promoting the translocation to the plasma membrane of the glucose transporter GLUT2 (in the case of liver) or GLUT4 (in the case of adipose tissue and muscle) **(Fig. 6)** [136, 137].

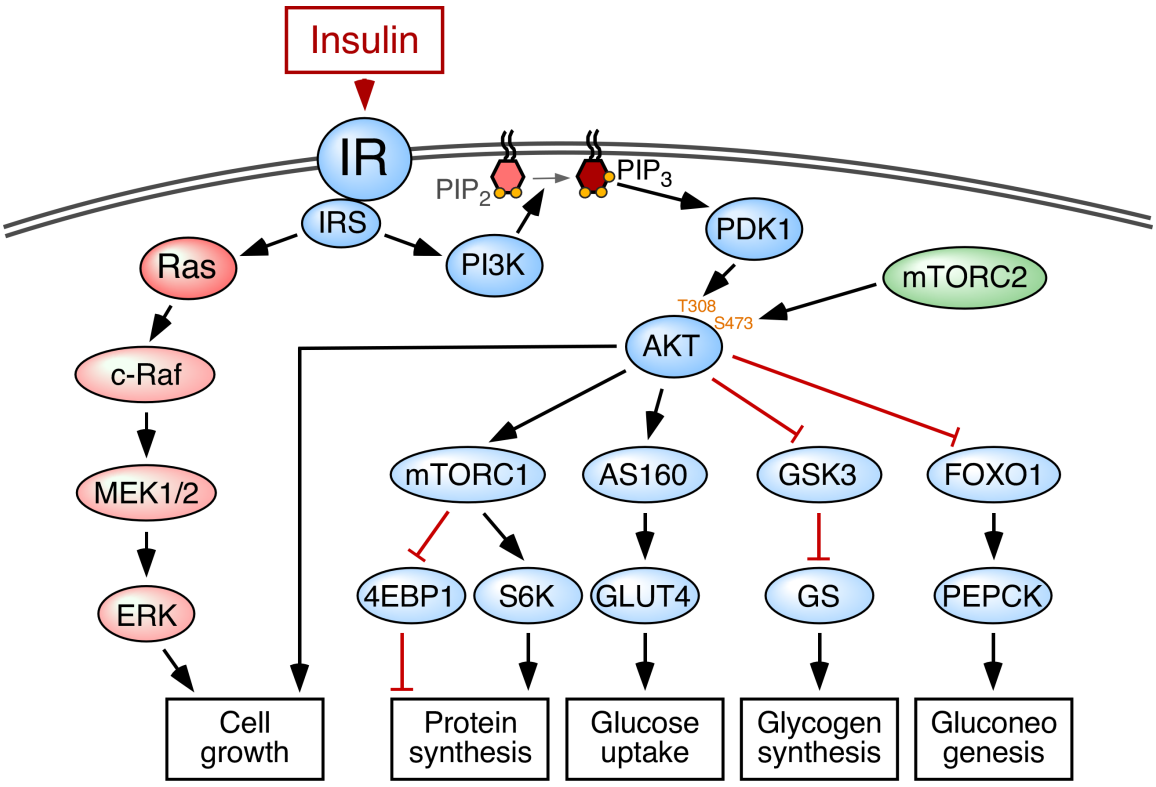

Figure 6. Insulin signaling pathway in skeletal muscle cells. IR, insulin receptor; MEK1/2, MAPK (mitogen-activated protein kinase)/ERK (extracellular signal-regulated kinase) kinase 1/2; ERK, extracellular signal-regulated kinase; PDK1, pyruvate dehydrogenase kinase 1; mTORC2, mammalian target of rapamycin complex 2; mTORC1, mammalian target of rapamycin complex 1; 4EBP1, 4E binding protein-1; S6K, p70 ribosomal protein S6 kinase; AS160, Akt substrate of 160 kDa; FOXO1, forkhead box protein O1; PEPCK, phosphoenolpyruvate carboxykinase. Other abbreviations have been described in the main text.

2.2 Skeletal muscle in glucose homeostasis

In addition to its intrinsic mechanical functions, skeletal muscle is responsible for ≈80% of the insulin-stimulated whole-body glucose uptake and clearance under normal physiological conditions [138, 139]. It also influences the metabolic status of other tissues such as WAT and BAT via the secretion of a large number of growth factors and hormones [138, 140, 141]. As a result, the improper function of this tissue can trigger the development of metabolic disorders such as type 2 diabetes and metabolic syndrome

[138, 139]. Given the extent of the contribution of this organ to glucose metabolism, the amount of muscle mass is also an important factor for metabolic homeostasis, as it has been demonstrated both in mice and humans [132, 142-144].

2.3 Rho GTPases in the regulation of glucose homeostasis

Rho GTPases have been implicated in glucose-stimulated insulin secretion and glucose uptake in both skeletal muscle and adipose tissue. Different studies in cells, rat and human islets have identified key roles for Rho, Rac1 and Cdc42 in pancreatic β–cells inducing cytoskeletal changes to promote the exocytosis of insulin granules [145]. It is also well established that Rac1 is necessary in skeletal muscle for Glut4 translocation to the plasma membrane upon the stimuli of insulin or contraction. In agreement with this, a recent study has even shown that type 2 diabetic patients exhibit lower Rac1 activation levels [146-150]. It is largely unknown how Rac1 is activated by insulin and there are discrepancies regarding the involvement of PI3K in the process [147, 151-154]. In adipose tissue, the GTPase TC10 is involved in the actin reorganization events needed for the translocation of GLUT4 to the plasma membrane [155]. Rho-kinase 1, a downstream effector of RhoA, has also been implicated in the positive regulation of insulin signaling in adipocytes and muscle cells through the serine phosphorylation of IRS–1 both *in vitro* and *in vivo* [156-158]. However, these results are controversial since adipose specific Rock1 deletion in mice causes enhanced insulin sensitivity. In addition, muscle–specific knock–in mice expressing a constitutively active version of Rock1 are insulin resistant [159, 160].

3. MUSCLE GROWTH AND PROTEOSTASIS

The regulation of muscle mass and fiber size during postnatal development reflects the protein turnover dynamics. Muscle hypertrophy occurs when the overall rates of protein synthesis exceed the rates of protein degradation. The opposite phenomenon applies in the case of muscle atrophy [161]. Moreover, in developing muscles the resident muscle stem cells undergo extensive proliferation, differentiation and fusion with the existent myofibers to increase the size of the muscle. Although at lower levels, this process can also be stimulated in adult skeletal muscle by specific stimuli, especially upon regenerative demands [161]. Several studies have shown that both processes contribute to muscle growth *in vivo*. However, the extent of the contribution of adult myogenesis to muscle mass alterations is still controversial [161-163].

3.1. Muscle mass and hypertrophy

The development and growth of the skeletal muscle is under the regulation of the insulin growth factor-1 (IGF-1) and, to a lesser extent insulin [136, 164-166]. The signaling pathway of the former is very similar to the explained for the latter (see **Fig. 6**). IGF-1 is recognized by the IGF-1 receptor promoting the recruitment and phosphorylation of IRS. As in the case of insulin, IRS triggers the stimulation of the PI3K-Akt pathway. The activation of this pathway modulates cell growth, differentiation, cell survival and protein synthesis [167]. In addition, IGF-1–mediated Foxo3 inhibition leads to the silencing of genes encoding E3 ubiquitin ligases, thus preventing the loss of muscle mass [168]. Skeletal muscle mass is controlled by additional mechanisms, such as the TGFβ family member myostatin [162, 164]. Extensive genetic data indicate that tampering with many of the above signaling elements cause muscle atrophy, insulin resistance, type 2 diabetes, and metabolic syndrome in the case of loss-of-function events. Conversely, gain-of-function changes in IGF-1 pathway elements, including IGF-1 itself, lead to muscle hypertrophy and protection against high fat diet (HFD)–triggered metabolic pathologies [132, 169, 170]. The same metabolic phenotype is observed when the muscle hypertrophy is triggered via inhibition of myostatin [132, 142, 171, 172].

3.2. Adult myogenesis

Adult muscle stem cells, also referred to as satellite cells, play a central role in the growth and regeneration of skeletal muscle. In vertebrates, these cells are located in a niche between the basal lamina and the sarcolemma [163]. Although mitotically quiescent, these cells can become activated upon stimulation by physical trauma or growth signals [163, 173]. After their activation, satellite cells enlarge their cytoplasm and re–start the cell cycle. They proliferate and undergo symmetric and asymmetric divisions to both renew the stem cell pool and give rise to intermediate cells committed to terminal differentiation, respectively. These cells, known as myoblasts, differentiate into myocytes that fuse to form the multinucleated myotubes that compose the myofibrils [173] **(Fig. 7)**.

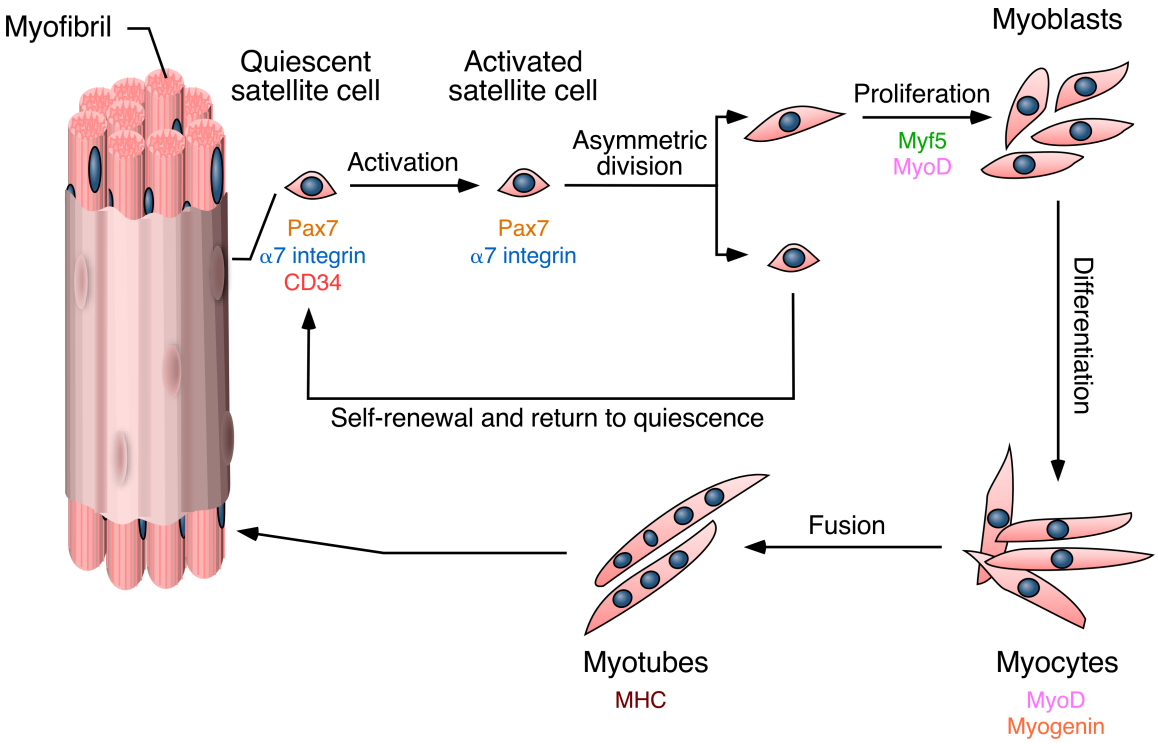

Figure 7. Muscle stem cells activation and differentiation processes. After a positive stimulus quiescent satellite cells become activated and lose the expression of the stem cell marker CD34. Activated satellite cells start to proliferate undergoing symmetric and asymmetric divisions to restore the stem cell pool and give rise to a proliferative population of myoblasts characterized by the expression of specific determination markers that trigger the differentiation process. The more mature cells named myocytes will fuse to form the myotubes which further elongate and mature into myofibers containing highly organized myofibrils.

The process of muscle differentiation is regulated by a number of transcription factors that are hierarchically activated along the differentiation process [174]. After the

MyoD–mediated transition to myocytes, the process of fusion into multinucleated myotubes is regulated by the late differentiation factors myogenic regulatory factor 4 and myogenin [174]. During the step of terminal differentiation, the myotubes activate the expression of specific myosin heavy chains (MHCs) that will define the type of muscle fiber and determine physiological characteristics such as the ATPase activity, contractibility and endurance **(Fig. 7)** [174].

3.3. Rho GTPases in myogenesis

Previous studies have shown that Rho GTPases play stepwise roles in skeletal myogenesis, although is not clear how their activation is controlled along this process. RhoA is necessary for the initial induction of the myogenic program, but its activity must be blocked for the fusion to take place [175-179]. By contrast, Rac1, Cdc42 and their effector proteins Pak1 and Pak3 are required for myoblast fusion, a differentiation step were extensive cytoskeletal rearrangements take place [180-184]. Previous studies have shown that a number of Rho GEFs intervene in the activation of Rac1 during the fusion step, namely Dock1, Dock5 and Trio. Dock1 is essential for primary myogenesis and myoblast fusion, being Dock5 nonessential and functionally redundant with the former [185-188]. Trio is activated by a M-Cadherin–dependent mechanism during the fusion step, but the myogenic defects in *Trio*$^{-/-}$ mice are different and less severe than the observed in *Dock1* knockout animals, suggesting that the Trio is only required during secondary fusion [180, 185, 189].

OBJECTIVES

1. To characterize the role of the lysine rich region in Vav1 signaling output.

2. To elucidate the role of lysine acetylation in the regulation of Vav1 activity.

3. To evaluate the involvement of Vav2 catalysis-dependent pathways in metabolic homeostasis.

METHODS

1. METHODS USED IN CHAPTERS 1 AND 2

1.1 Mammalian expression vectors

All the Vav family constructs used in this work encode versions of the murine species and were DNA sequence–verified in our Genomics Facility. Plasmids expressing Vav1^{WT} (pJLZ52), Vav1$^{\Delta 1–186}$ (pMJC10), Vav1^{Y174E} (pMB123), EGFP–Vav1^{WT} (pSRM3), EGFP–Vav1$^{\Delta 1–186}$ (pNM108), EGFP–Vav1$^{\Delta 835–845}$ (pMB6), and His–tagged Vav2^{WT} (pAO1) were previously described [21, 23, 27, 28, 31, 190]. The pNFAT–Luc, the pSRE–luc and the pC.HA Vav3 (Vav3^{WT}) plasmids were obtained from Addgene, the pFR–Luc and pFA2–cJun plasmids from Stratagene (now, Agilent Technologies), and the pRL–SV40 plasmid from Promega. The plasmids encoding the pmRFP (pmRFP–Ruby–Lifeact) and the two IpgD versions (pRK5–Myc–IpgD and pRK5–Myc–IpgD–C438S) were obtained from M.A. del Pozo (Centro Nacional de Investigaciones Cardiovasculares, Madrid, Spain) and B. Payrastre (INSERM U1048, Toulouse, France), respectively.

The rest of the plasmids encoding Vav1 mutant proteins were generated in this work by site–directed mutagenesis using the high–fidelity NZYProof DNA polymerase (Cat. #14601, NZYTech) and the appropriate combination of mutation–bearing oligonucleotides **(Table 1)**. The generation of the plasmids encoding the Vav1 KR1^{Mut} (pSRF10) and KR2^{Mut} (pSRF9) mutants required a two–step site–directed mutagenesis strategy. In the first step, we deleted (in the case of KR1^{Mut}) or inserted (in the case of KR1^{Mut}) a single nucleotide before the first codon of the nucleotide sequence that we want to mutate. The second mutagenesis step involved the insertion (in the case of KR1^{Mut}) and deletion (in the case of KR1^{Mut}) of a nucleotide to recover the reading frame at the end of the region that was mutated. In all these cases, the pJLZ52 plasmid was used as first DNA template for the PCR reaction. The plasmids encoding Vav1 Δ835–845+KR1^{Mut} (pSRF79) and Vav1 Δ835–845+KR2^{Mut} (pSRF37) were generated as above using the pSRF49 plasmid as template. The vectors encoding Vav1 Δ1–186+KR1^{Mut} (pSRF23) and Vav1 Δ1–186+KR2^{Mut} were generated as above using the pMJC10 plasmid as template. The expression vectors encoding Vav1$^{\Delta 835–845}$ (pSRF49), Vav1^{E591K} (pSRF41), Vav1^{E598K} (pSRF40) and Vav1^{G691V} (pSRF46) were generated using the oligonucleotides shown in **Table 1** and the pJLZ52 plasmid as template. The vectors encoding Vav1$^{E591K+E5988K}$ (pSRF88) and Vav1^{3xEK} (pSRF97) were generated using the indicated nucleotides **(Table 1)** and the plasmids pSRF41 and pSRF88 as templates,

respectively.

To generate the plasmids encoding EGFP–tagged Vav1 KR^{Mut}, the vectors pSRF10 and pSRF9 were digested with KpnI and EcoRI to liberate a fragment of the mouse *Vav1* cDNA encoding the KR region. Upon purification, the cDNA fragment was ligated into the appropriate Vav1–encoding expression vector that was previously linearized with KpnI and EcoRI. Specifically, the KpnI–EcoRI fragments used to generate the EGFP–Vav1 $KR1^{Mut}$ (pSRF20) and EGFP–Vav1 $KR2^{Mut}$ (pSRF17) encoding vectors were liberated from the pSRM3 plasmid, those for the EGFP–Vav1 Δ1–186+$KR1^{Mut}$ (pSRF21) and EGFP–Vav1 Δ1–186+$KR2^{Mut}$ (pSRF18) from pNM108, and those for EGFP–Vav1 Δ835–845+$KR1^{Mut}$ (pSRF22) and EGFP–Vav1 Δ835–845+$KR2^{Mut}$ (pSRF19) from pMB6.

For the generation of the plasmid encoding the His–tagged Vav2+KR^{Vav1} chimera, we used a synthetic double stranded DNA flanked by KpnI and XbaI sites (Cat. 16AB33NC_1918158, Thermo Fisher Scientific) that encoded an altered version of Vav2 in which its amino acids 572 to 588 were replaced by the *Vav1* sequence encoding the amino acid sequence between the 564 and the 604 residues. The sequence was then cloned into the KpnI–XbaI–linearized pAO1 plasmid that encoded the full–length Vav2 protein.

The plasmid encoding $Vav1^{CAAX}$ (pSRF93) was obtained in two mutagenic steps. The first one involved an inverse PCR using pJLZ52 as template and the primers shown in **Table 1** to introduce the most C–terminal sequence (CVLS) of the H–Ras CAAX box. In the second step, the nucleotides encoding the sequence most H–Ras amino acids located N–terminally to the CVLS box (CMSCK) were inserted via a site–directed insertional mutagenesis approach using the former plasmid as template and the second pair of primers indicated in **Table 1**. The plasmids encoding Vav1 $KR1^{Mut+CAAX}$ (pSRF98) and $Vav1^{G691V+CAAX}$ (pSRF96) were obtained by site–directed mutagenesis using the pSRF93 as template and the indicated primers **(Table 1)**.

The rest of the plasmids encoding Vav1 mutant proteins were generated in this work by site–directed mutagenesis using the combination of mutation–bearing primers indicated in the **Table 2**. The plasmids pJLZ52, pSRF49, pMJC10 and pSRF93 were used as templates in the case of plasmids encoding mutant versions of Vav1, pAO1 in the case of Vav2 and pC.HA Vav3 in the case of Vav3.

TABLE 1. Sequence of oligonucleotides used in this study

Mutant	DNA sequence of primer	
KR1^{Mut}	F_1*	5'– CAAGATTTCGCAGGAACCAT(G)GAAGAAGGACAAGCTCCATC –3'
	R_1	5'– GATGGAGCTTGTCCTTCTTC(C)ATGGTTCCTGCGAAATCTTG –3'
	F_2	5'– GGACAAGCTCCATCG–AGGGCCCAGGACAAG –3'
	R_2	5'– CTTGTCCTGGGCCCT–CGATGGAGCTTGTCC –3'
KR2^{Mut}	F_1	5'– CATCGAAGGGCCCAGGAC–AGAAAAGGAATGAATTGGG –3'
	R_1	5'– CCCAATTCATTCCTTTTCT–GTCCTGGGCCCTTCGATG –3'
	F_2	5'– TCTGCCTAAGATGGAAGTGTTT(T)CAGGAATACTATGGGATCCCTC –3'
	R_2	5'– GAGGGATCCCATAGTATTCCTG(A)AAACACTTCCATCTTAGGCAGA –3'
CAAX	F_1	5'– GCCTGGTGCCCTGTAGGACACAGCGAG –3'
	R_1	5'– [p]–GCTCTAGATCAGGAGAGGACGCAGCAATATTCGGAATAGTCTTCC –3'
	F_2	5'– GGAAGACTATTCCGAATATTGCTGTATGTCATGTAAGTGCGTCCTCTCCTG ATCTAGAGC –3'
	R_2	5'– GCTCTAGATCAGGAGAGGACGCACTTACATGACATACAGCAATATTCGGA ATAGTCTTCC –3'
Δ835–845	F	5'– CCCTTCTAACTAAGTGGAGGAAGAC –3'
	R	5'– GTCTTCCTCCACTTAGTTAGAAGGG –3'
D578K	F	5'– CGCAGGAACCATGAAGAAGAAAAAGCTCCATCGAAGGGCCC –3'
	R	5'– GGGCCCTTCGATGGAGCTTTTTCTTCTTCATGGTTCCTGCG –3'
E591K	F	5'– CCCAGGACAAGAAAAGGAATAAATTGGGTCTGCCTAAGATG –3'
	R	5'– CATCTTAGGCAGACCCAATTTATTCCTTTTCTTGTCCTGGG –3'
E598K	F	5'– GGGTCTGCCTAAGATGAAAGTGTTTCAGGAATAC –3'
	R	5'– GTATTCCTGAAACACTTTCATCTTAGGCAGACCC –3'
G691V	F	5'– CCAACCGTTCTGATGTGACCTATCTGGTGCG –3'
	R	5'– CGCACCAGATAGGTCACATCAGAACGGTTGG –3'
MBP–C1	F	5'– GCAGGAACCATGTAGAAGGACAAGC –3'
	R	5'– GCTTGTCCTTCTACATGGTTCCTGC –3'
MBP–KR	F	5'– CCTATAGATCTGGTCGCCATGGGCAAGATTTCGC –3'
	R	5'– GGAGGAGGGATCCCATAGTATTCC –3'
PH^{Mut} (R422A)	F	5'– CGCTCAAAGACAGACGCGTATGCCTTCCTGCTG –3'
	R	5'– CAGCAGGAAGGCATACGCGTCTGTCTTTGAGCG –3'
C1^{Mut} (L536G)	F	5'– AGGGCCTGCCAGATGTTAGGCAGAGGCACATTCTACCAG –3'
	R	5'– CTGGTAGAATGTGCCTCTGCCTAACATCTGGCAGGCCCT –3'

*F, forward primer (in the case of a two–step mutagenesis protocol, the primers are referred to as F_1 and F_2 for the first and second step, respectively); R, reverse primer (in the case of a two–step mutagenesis protocol, the primers are referred to as R_1 and R_2 for the first and second step, respectively); [p]–, phosphorylated primer. Nucleotides used for the generation of the indicated mutations are shown in red. Nucleotides that have been inserted or deleted in the WT sequence are indicated in red parenthesis and with a red line, respectively.

TABLE 2. Sequence of oligonucleotides used in the acetylation study (continues in next page)

Mutant	DNA sequence of primer	
Vav1^{K194R}	F*	5'– CAGAGTATGATAGGCGCTGCTGCTG –3'
	R	5'– CAGCAGCAGCGCCTATCATACTCTG –3'
Vav1^{K194Q}	F	5'– GACAGAGTATGATCAGCGCTGCTGCTG –3'
	R	5'– CAGCAGCAGCGCTGATCATACTCTGTC –3'
Vav1^{K222R}	F	5'– CAGCAGCACTTCATGAGGCCTCTGCAGCTATTC –3'
	R	5'– GAATCGCTGCAGAGGCCTCATGAAGTGCTGCTG–3'
Vav1^{K222Q}	F	5'– CAGCACTTCATGCAGCCTCTGCAGC –3'
	R	5'– GCTGCAGAGGCTGCATGAAGTGCTG –3'
Vav1^{K252R}	F	5'– GCATACCCACTTCTTAAGGGAACTGAAGGATGCCC –3'
	R	5'– GGGCATCCTTCAGTTCCCTTAAGAAGTGGGTATGC–3'
Vav1^{K252Q}	F	5'– GCATACCCACTTCTTACAGGAACTGAAGGATGC –3'
	R	5'– GCATCCTTCAGTTCCTGTAAGAAGTGGGTATGC –3'
Vav1^{K335R}	F	5'– ATGCAGCGGGTGCTGAGGTACCACCTCCTTCTC –3'
	R	5'– GAGAAGGAGGTGGTACCTCAGCACCCGCTGCAT–3'
Vav1^{K335Q}	F	5'– CCTATGCAGCGGGTGCTGCAGTACCACCTCCTTCTCC –3'
	R	5'– GGAGAAGGAGGTGGTACTGCAGCACCCGCTGCATAGG –3'
Vav1^{K374R}	F	5'– TGCGTGAACGAGGTCAGGAGGGACAATGAAACC–3'
	R	5'– GGTTTCATTGTCCCTCCTGACCTCGTTCACGCA –3'
Vav1^{K374Q}	F	5'– GTGCGTGAACGAGGTCCAGAGGGACAATGAAAC –3'
	R	5'– GTTTCATTGTCCCTCTGGACCTCGTTCACGCAC –3'
Vav1^{K587R}	F	5'– GGCCCAGGACAGGAAAAGGAATG –3'
	R	5'– CATTCCTTTTCCTGTCCTGGGCC –3'
Vav1^{K587Q}	F	5'– GGGCCCAGGACCAGAAAAGGAATG –3'
	R	5'– CATTCCTTTTCTGGTCCTGGGCCC –3'
Vav1^{K588R}	F	5'– GGCCCAGGACAAGAGAAGGAATGAATTGG –3'
	R	5'– CCAATTCATTCCTTCTCTTGTCCTGGGCC –3'
Vav1^{K588Q}	F	5'– GGGCCCAGGACAAGCAAAGGAATGAATTG –3'
	R	5'– CAATTCATTCCTTTGCTTGTCCTGGGCCC –3'
Vav1^{K716R}	F	5'– CAGCATTAAGTATAACGTGGAGGTCAGGCATATTAAAATCATGACGTCAGA –3'
	R	5'– CCTCTGACGTCATGATTTTAATATGCCTGACCTCCACGTTATACTTAATGC–3'
Vav1^{K716Q}	F	5'– CATTAAGTATAACGTGGAGGTCCAGCATATTAAAATCATGACGTC –3'
	R	5'– GACGTCATGATTTTAATATGCTGGACCTCCACGTTATACTTAATG –3'
Vav1^{K782R}	F	5'– CAGCTGGAAGCACCAGGTATTTTGGCACTGC –3'
	R	5'– GCAGTGCCAAAATACCTGGTGCTTCCAGCTG –3'
Vav1^{K782Q}	F	5'– CCAGCTGGAAGCACCCAGTATTTTGGCACTG –3'
	R	5'– CAGTGCCAAAATACTGGGTGCTTCCAGCTGG –3'
Vav1^{K815R}	F	5'– GATCCTCAATAAGAGGGACAGCAAGGC –3'
	R	5'– GCCTTGCTGTCCCCTCTTATTGAGGATC –3'
Vav1^{K815Q}	F	5'– GATCCTCAATAAGCAGGGACAGCAAGG –3'
	R	5'– CCTTGCTGTCCCTGCTTATTGAGGATC –3'
Vav2^{K718R}	F	5'– CAATGATGAGGTGAGACATATCAAGGTGG –3'
	R	5'– CCACCTTGATATGTCTCACCTCATCATTG –3'
Vav2^{K718Q}	F	5'– GTTCAATGATGAGGTGCAACATATCAAGGTGG –3'
	R	5'– CCACCTTGATATGTTGCACCTCATCATTGAAC –3'

TABLE 2. Sequence of oligonucleotides used in the acetylation study (continuation from previous page)

Mutant		DNA sequence of primer
Vav3^{K717R}	F	5'– GTACAATAATGAAGCAAGGCACATCAAGATTTTAAC –3'
	R	5'– GTTAAAATCTTGATGTGCCTTGCTTCATTATTGTAC –3'
Vav3^{K717Q}	F	5'– CAATAATGAAGCACAGCACATCAAG –3'
	R	5'– CTTGATGTGCTGTGCTTCATTATTG –3'

*F, forward primer; R, reverse primer. Nucleotides used for the generation of the indicated mutations are shown in red.

1.2 Bacterial expression vectors

The plasmids encoding MBP–Vav1 DH–PH–C1–KR (pXRB7), MBP–Vav1 PH (pJLZ2), MBP–Vav1 C1–KR (pXRB1), and MBP–Vav3 C1–KRL (pNM128) were described before [21, 27, 28]. The bacterial expression plasmid encoding the MBP–Vav1 C1 (pSRF120) was obtained by introducing a stop codon after the residue 570 of Vav1 by site–directed mutagenesis using the primers indicated in **Table 1** and the pXRB1 template. To generate the plasmid encoding the MBP–Vav1 KR (SRF126), a *Vav1* cDNA fragment encoding the KR flanked by BglII and BamHI restriction sites was PCR–amplified from the pJLZ52 vector using the primers indicated in **Table 1** and, upon purification, cloned into the BamHI–linearized pMAL–c vector (New England Biolabs). The plasmids encoding MBP–Vav1 C1–KR1^{Mut} (pSRF149) and MBP–Vav1 C1–KR^{3xEK} (pSRF148) were generated using the plasmid pXRB1 as template and the mutagenesis strategies described above for the generation of the analogous mutations in full–length Vav1. The same strategy was used to generate the vectors encoding MBP–Vav1 KR1^{Mut} (pSRF137) and MBP–Vav1 KR^{3xEK} (pSRF144) although, in this case, we utilized the pSRF126 plasmid as template.

1.3 Immunological reagents

The homemade polyclonal antibody to the Vav1 DH domain (Ref. 302–5), phosphoY174 (Ref. 613), phosphoY280 (Ref. 595) and phosphoY836 (Ref. 622) were raised in rabbits and described elsewhere [21, 30, 31]. Other antibodies used in this study include those recognizing human CD3 (UCHT1 clone, Cat. #217570; Merk–Millipore), tubulin α (Cat. #CP06; Calbiochem), polyhistidine (Cat. #H–1029; Sigma), chicken IgM (Cat. #8300–

01; Southern Biotech), MBP (Cat. #M–6295; Sigma), GST (Cat. #G1160; Sigma), Vav1 (D-7) (Cat. #sc-8039; Santa Cruz Biotechnology), phosphotyrosine (PY99) (Cat. #sc-7020; Santa Cruz Biotechnology), acetyl-lysine (Cat. #AB3879; Chemicon), CD98 (Cat. #ab108300; Abcam), HA (Cat. #5017; Cell Signaling) and GAPDH (Cat. #sc-25778; Santa Cruz Biotechnology). Rhodamine–labeled phalloidin (Cat. #PHDR1) was obtained from Cytoskeleton.

1.4 Phylogenetic and conservation analyses

Amino acid sequences from Vav family proteins were obtained from the UniProt database (National Center for Biotechnology Information, Bethesda, MD) and aligned using the multiple sequence alignment by log–expectation algorithm [191, 192] in the Jalview software [193]. The PhyML software was used to build the phylogenetic trees based on the maximum–likelihood principle [194].

1.5 Calculation of the isoelectric point

Isoelectric points were calculated using the ExPASy ProtParam (Swiss Institute of Bioinformatics).

1.6 Cell culture and treatments

Jurkat and Raji cells were obtained from the ATCC and grown in RPMI–1640 medium supplemented with 10% fetal calf serum, 1% L–glutamine, penicillin (10 µg/ml) and streptomycin (100 µg/ml). DT40 cells were obtained from the Riken Bioresource Center (Ibaraki, Japan) and grown in RPMI–1640 medium supplemented with 10% fetal calf serum, 1% chicken serum, 0.1 mM β–mercaptoethanol, 1% L–glutamine, penicillin (10 µg/ml) and streptomycin (100 µg/ml). COS1 cells were grown in DMEM supplemented with 10% fetal calf serum, 1% L–glutamine, penicillin (10 µg/ml) and streptomycin (100 µg/ml). All tissue culture reagents were obtained from Gibco. All cell lines were maintained at 37ºC and a 5% CO2 humidified atmosphere. When required, cells were stimulated for the indicated periods of time with antibodies to human CD3 (7.5 µg/mL), chicken IgM (5 µg/ml) and EGF (50 ng/mL, Cat. number E9644, Sigma; COS1 cells). In the latter case, cells were previously starved without serum for 3 hours.

1.7 Luciferase reporter assays

Exponentially growing Jurkat (2 x 10^7 cells per condition) and DT40 cells (1 x 10^7 cells per condition) were electroporated (250V, 950 μF pulses) using a Gene Pulser II apparatus (Cat. #165–2106; BioRad). In the case of JNK assays, the cells were electroporated with the firefly luciferase reporter pFR–Luc (5 μg), pFA2–c–Jun (2 μg), a vector constitutively expressing the Renilla luciferase (pRL–SV40, 10 ng), and 20 μg of the indicated expression vector. When two experimental plasmids were introduced, 10 μg of each plasmid were electroporated in order to maintain constant the total amount of transfected plasmids. In the case of NF–AT assays, the cells were electroporated with 3 μg of a luciferase reporter plasmid containing three NFAT binding sites (pNF–AT/luc), 10 ng of pRL–SV40, and the indicated experimental plasmids as above. When required, empty plasmids were included in the electroporations to maintain constant the total amount of DNA introduced in cells among all the experimental samples. After 36 hours in complete medium, the electroporated cells were either left untreated or stimulated with the indicated antibodies for seven hours. Cells were then washed in serum–free media, lysed in Passive Lysis Buffer (Cat. #E1960; Promega), and the luciferase activity obtained in each condition recorded using the Dual–Luciferase Reporter System (Cat. #E1960; Promega) according to the supplier's recommendations in a Lumat LB 9507 luminometer (Berthold). The raw values obtained were normalized according to the activity of the *Renilla* luciferase recorded in each sample. Final values are represented as the fold–change of the normalized luciferase activity obtained when compared to the control sample. In the case of experiments using COS1 cells, we transfected 1 x 10^6 exponentially growing cells with 1 μg of pSRE–luc, 1 ng of pRL–SV40, and 1 μg of the appropriate experimental vectors using Lipofectamine 2000 (Cat. #11668019; Invitrogen). Cells were cultured in complete medium for 36 hours, washed, lysed, and luciferase activities determined as indicated above. In all cases, the abundance of the ectopically expressed proteins under each experimental condition was verified by analyzing aliquots of the cell extracts used in the luciferase experiments by immunoblot.

1.8 Western blotting

Protein samples were denatured by boiling in SDS-PAGE Laemmli buffer, separated electrophoretically and transferred onto nitrocellulose filters using the iBlot Dry Blotting

System (Invitrogen) according the manufacturer's protocol. Membranes were blocked in 5% bovine serum albumin (Cat. #A4503; Sigma) in TBS-T (25 mM Tris–HCl [pH 8.0], 150 mM NaCl, 0.1 % Tween–20) for 1 h and then incubated overnight at 4 ºC with the appropriate primary antibodies diluted in blocking buffer. After three washes with TBS-T, the membrane was incubated with horseradish peroxidase-conjugated Protein A or the appropriate secondary antibody (1:5,000 dilution) for 45 min at room temperature. Immunoreacting bands were developed using a standard chemoluminescent method (ECL; Cat. #32106, Pierce).

1.9 Immunofluorescence

Liposome–transfected COS-1 cells (Lipofectamine 2000, Cat. #11668019; Invitrogen) were fixed in 4 % formaldehyde in a phosphate–buffered saline solution (PBS) for 15 min, washed twice with PBS, permeabilized with 0.5 % Triton X–100 in TBS–T for 10 min, washed three times with TBS–T, blocked in TBS–T supplemented with 2% bovine serum albumin (Cat. #A4503; Sigma) for 30 min, incubated with anti-Vav (DH) (1:400) for 2 hours, washed three times with TBS–T, incubated with Alexa Fluor 488-conjugated anti-rabbit IgG (1:400; Cat. #A-21206; Molecular Probes) for 50 minutes, washed three times with TBS–T, incubated with rhodamine–labeled phalloidin (Cat. #PHDR1; Cytoskeleton) diluted 1:200 in blocking solution for 20 min, washed three times in TBS–T and finally mounted onto microscope slides using Mowiol (Cat. #9002–89–5; Calbiochem). Microscopic analysis was performed using a Leica DM 6000B fluorescence microscope and a Hamamatsu ORCA-ER C4742-80 camera (Hamamatsu, Hamamatsu, Japan).

1.10 Confocal microscopy analyses

Liposome–transfected COS1 cells were fixed in 4 % formaldehyde in a phosphate–buffered saline solution (PBS) for 15 min, washed twice with PBS, permeabilized with 0.5 % Triton X–100 (Cat. #T8787; Sigma) in TBS–T for 10 min, washed three times with TBS–T, blocked in TBS–T supplemented with 2 % bovine serum albumin for 30 min, incubated with rhodamine–labeled phalloidin (diluted 1:200 in blocking solution) for 20 min, washed three times in TBS–T and, finally, stained with 1 µg/ml of 4',6–diamidino–2–phenylindole (Cat. #D1306; Invitrogen) for 5 min to visualize the nuclei. In

the case of nonconjugated Jurkat cells, 2 x 10^6 cells were transfected with the Program #5 of the Neon transfection system (Cat. #MPK5000; Invitrogen) according to the manufacturer's instructions. After 36 hours, the cells were washed in RPMI–1640 medium, plated onto 12–mm–diameter poly–D–lysine–coated coverslips (Cat. #354086; Corning BioCoat), and allowed to settle for 15 min. Cells were then fixed for 10 min with 4% paraformaldehyde in PBS, washed twice with PBS, permeabilized for 15 min in 0.5% Triton X–100 in TBS–T, washed again as above, and blocked in 2% bovine serum albumin in TBS–T for at least 15 min. The cells were then incubated for 20 min in a wet–chamber with a 1:200 dilution of rhodamine–labeled phalloidin in blocking buffer, washed three times with TBS–T, and stained with 4',6–diamidino–2–phenylindole as above. In all cases, the stained preparations were mounted onto microscope slides using Mowiol (Cat. #9002–89–5; Calbiochem). Images were acquired using a Leica TCS SP5 confocal microscope and processed using the LAS AF software (version 2.6.0.72266, Leica).

For immune synapse studies, Jurkat cells were transfected as above and, after 36 hours, washed with RPMI–1640 medium and then gently mixed with an equal number of Raji cells that had been previously incubated in the presence of both 0.5 µg/ml of superantigen E (Cat. #ET404; Toxin Technology) and 10 µM of the 7–amino–4–chloromethylcoumarin membrane permeable cell tracker (Cat. #C2110; Invitrogen) for 1 hour at 37ºC in serum free media. After 15 min, cells were plated on 12–mm–diameter, poly–D–lysine–coated coverslips, allowed to settle, and further processed for microscopy analyses as indicated above.

For the experiments using live cells, the Jurkat cells were transfected with 30 µg of the appropriate Vav1–encoding expression plasmid plus 15 µg of pmCherry–LifeAct. After 36 hours, cells were washed in RPMI–1640 medium, and allowed to adhere onto poly–L–lysine coated coverslips (1:100 dilution incubated overnight). Upon mounting the coverslips onto Attofluor open chambers (Cat. #A7816; Invitrogen), the cells were maintained in 500 µl of RPMI–1640 medium at 37°C on the microscope stage. Upon addition of equal numbers of superantigen E–loaded Raji cells to the chambers, the formation of Jurkat–Raji conjugates was recorded using a TCS SP5 confocal microscope (Leica) and images processed using the LAS AF software (version 2.6.0.72266, Leica).

For the immunostaining of Vav1 in COS1 cells, blocked samples were incubated with anti-Vav (DH) (1:400) for 2 hours, washed three times with TBS–T, incubated with Alexa Fluor 488-conjugated anti-rabbit IgG (1:400; Cat. #A-21206; Molecular Probes)

for 50 minutes, washed three times with TBS–T, incubated with rhodamine–labeled phalloidin (Cat. #PHDR1; Cytoskeleton) diluted 1:200 in blocking solution for 20 min, washed three times in TBS–T and finally mounted onto microscope slides using Mowiol (Cat. #9002–89–5; Calbiochem). In this case, microscopic analysis was performed using a Leica DM 6000B fluorescence microscope and a Hamamatsu ORCA-ER C4742-80 camera (Hamamatsu, Hamamatsu, Japan).

1.11 Quantification of confocal images

Profiles of fluorescence intensity and levels of protein colocalization along the indicated axes of the cell images were obtained using the ImageJ software (National Institutes of Health, Bethesda, MD). The ratio of Vav1 protein at the plasma membrane was calculated creating a mask with the phalloidin staining to discriminate between the fluorescence of Vav1 at the membrane (coincident with phalloidin–positive structures) and the cytoplasmic fraction (noncoincident with phalloidin–positive F–actin). The orthogonal reconstruction of the contact area between Jurkat–Raji conjugates was carried out using the 3D module of the LAS X software (Leica). The polymerization of F–actin was determined using the ImageJ plug–in previously described [195]. In brief, the rhodamine–phalloidin fluorescence present in either the contact area (inside) or the adjacent area (outside) of the immune synapse was compared with nonengaged membrane areas of both the T cell and the superantigen–presenting cell membrane. The same approach was used to calculate Vav1 polarization to the immune synapse, comparing the fluorescence within the contact area to the signal in other areas of the T cell.

1.12 Purification of MBP fusion proteins

Exponentially growing cultures of *E. coli* DH5α cells were treated with isopropyl β–D–1–thiogalactopyranoside (Cat. # I5502; Sigma) at 25 °C for 90 min, centrifuged at 6,000 rpm for 10 min at 4ºC and resuspended in lysis buffer [10 mM sodium phosphate, 0.25% (w/w) Tween-20, 30 mM NaCl, 10 mM β–mercaptoethanol, 10 mM EDTA, 10 mM EGTA]. The samples were frozen overnight, thawed in ice, disrupted by sonication on ice, centrifuged again, and the supernatant containing the MBPs subjected to purification using an amylose resin (Cat. #E8021; New England Biolabs). The MBPs were eluted with 5 ml of 10 mM maltose in column buffer (20 mM Tris–HCl, 200 mM NaCl, 1 mM

EDTA, pH 7.4) and 500 µl fractions were serially collected. Proteins were conserved at –20ºC until further use. Protein concentration was quantified on polyacrylamide gels using known concentrations of bovine serum albumin as standard.

1.13 Phospholipid binding assays

Membranes with spotted phospholipids (PIP strips, Cat. #P–6001; PIP arrays, Cat. #P6100; Echelon Biosciencies) were blocked for 1 hour in blocking buffer (1% nonfat–dry milk in phosphate–buffered saline solution) at room temperature, incubated overnight with either 1 µg/ml (in the case of PIP strips) or 0.5 µg/ml (in the case of PIP arrays) of the indicated MBPs in blocking buffer at 4 °C, washed three times in PBS–T (phosphate–buffered saline containing 0.1 % Tween–20), incubated with an antibody to MBP (1:3000 dilution) in PBS–T for one hour at 4 °C, washed three times in PBS–T, and incubated with the secondary antibody for one hour in PBS–T. After three serial washes with PBS–T, the protein bound to the lipids was detected by chemoluminiscence (Pierce ECL, Cat. #32106; Thermo Fisher Scientific). The blots with the control GST–PLC– δ1 PH fusion proteins (provided by Echelon Biosciences) were done as above with the exception of the primary antibody used to detect the protein. The dot blots were scanned in ImageJ and the results fitted into a five–parameter nonlinear regression model using the GraphPad Prism software (version 6.0).

1.14 Alignment of amino acid sequences

The appropriate amino acid sequences of the indicated proteins were obtained from the UniProt (National Center for Biotechnology Information, Bethesda, MD) or the Simple Modular Architecture Research Tool (SMART) database [196] and aligned using Jalview.

1.15 Immunoprecipitation

In the case of COS1 cells, we ectopically expressed the indicated proteins using the diethylaminoethyl-dextran (10 mg/mL, Cat. #D9885, Sigma)/chloroquine (2.5 mM, Cat. #C6628, Sigma) method [197]. Two 10-cm diameter plates were transfected per condition using 10 µg of plasmid per plate. 48 hours post-transfections, cells were washed in a phosphate-buffered saline (PBS) solution and lysed with the aid of a scrapper in 1 mL of RIPA buffer [10 mM Tris-HCl (pH 7.5), 150 mM NaCl, 1% Triton

X-100 (Cat. number X100, Sigma), 1 mM Na_3VO_4 (Cat. number S6508, Sigma), 1 mM NaF (Cat. number S7920, Sigma) and the Cømplete protease inhibitor cocktail (Cat. number 11836145001, Roche)]. Cellular extracts were kept 5 min on ice and subsequently centrifuged at 14 000 rpm for 10 min at 4 ºC to eliminate cell debri. The supernatants were then incubated with either 7 µL of an antibody to Vav1 or 5 µL of an antibody to acetylated lysines overnight at 4 ºC. Immunocomplexes were then collected with Gammabind G-Sepharose beads (Cat. number GE17-0885-01, GE Healthcare), washed three times in RIPA buffer, resuspended in SDS-PAGE buffer, boiled for 5 min, electrophoresed, and subjected to immunoblot analyses with the indicated antibodies.

In the case of Jurkat, 10×10^6 cells were transfected with 20 µg of DNA per condition using the Program #5 of the Neon transfection system (Cat. number MPK5000, Invitrogen) according to the manufacturer's instructions. After 48 hours, the cells were washed, transferred to a 1.5 mL Eppendorf tube and, after low speed centrifugation at 4 ºC, resuspended in lysis buffer with extensive vortexing. The cell extracts obtained processed as above. However, in the case of immunoprecipitation experiments using GFP-Vav1, the cell lysates were incubated with the GFP-Trap reagent (Cat. number gta-100, ChromoTek) for 1 hour at 4 ºC. Washed immunocomplexes were collected by centrifugation and subjected to immunoblot analyses as above. In all cases, total cellular lysates were analyzed in parallel to monitor the expression of the ectopically expressed proteins used in each experiment. In all cases analyses of total cellular lysates were performed in parallel to detect the expression of the indicated proteins.

1.16 Subcellular fractionation

20×10^6 exponentially growing Jurkat cells were electroporated when indicated as for luciferase reporter assays. After 24 hours, cells were either left nonstimulated or stimulated with anti–CD3 for 2 minutes. Cells were then centrifuged, resuspended in 1 ml of hypotonic buffer [10 mM Tris–HCl (pH 7.5), 38 mM sodium chloride, 1 mM sodium orthovanadate, 1 mM sodium fluoride and cØmplete Protease Inhibitor Cocktail] and kept on ice for 5 min. After 5 freeze/thaw cycles (4 min at –80º C and 20 sec at 42º C), cells were centrifuged at 14 000 rpm for 10 min at 4°C and the pellets discarded. The supernatants were then centrifuged in an ultracentrifuge (Optima TL Ultracentrifuge; Beckman Coulter) at 60 000 rpm for 1 hour at 4 °C using polycarbonate centrifuge tubes (Cat. #349622; Beckman Coulter). The supernatant was considered as the cytoplasmic

compartment and Triton X–100 was added to a final 1% concentration. The pellet was resuspended again in hypotonic buffer and centrifuged as above. This new pellet was resuspended in hypotonic buffer with 1% Triton X–100 to obtain the plasma membrane fraction. SDS–PAGE buffer was added to all the samples, boiled for 5 min, and analyzed by immunoblot as indicated above.

1.17 Mass spectrometric analysis

Upon the GFP-trap–mediated immunoprecipitation, the GFP-Vav1 proteins were separated by one-dimensional SDS–PAGE electrophoresis and Coomassie blue–stained. The area of the gel containing the GFP–Vav1 (according to molecular weight mobility) was excised and subjected to in-gel digestion with trypsin following a modified protocol from Shevchenko et al. [198]. To this end, the gel pieces were destained at 37ºC for 15 min using a solution of 50% acetonitrile in 50 mM sodium bicarbonate. Subsequently, the protein reduction and alkylation steps were performed using 10 mM DTT (56 ºC, 45 min) and 55 mM iodoacetamide (room temperature, 30 min). Upon digestion with trypsin (6.25 ng/mL) at 37 ºC for 18 hours, the peptide-containing solutions were acidified with formic acid (FA) and desalted by using C18-Stage-Tips columns [199], partially dried, and stored at –20 ºC. For mass spectrometry analysis, the peptides were dissolved in 0.5% FA/3% acetonitrile (ACN), loaded onto a trapping column (nanoACQUITY UPLC 2G-V/M Trap Symmetry 5 µm particle size, 180 µm × 20 mm C18 column; Cat. number 186006527, Waters Corp., Milford/MA, USA), and separated using a nanoACQUITY UPLC BEH C18 column (1.7 µm, 130 Å and a 75 µm × 250 mm; Cat. number 186003545, Waters Corp., Milford/MA, USA) at 40ºC and with a linear gradient ranging from 7 to 35% of solvent B (ACN/0.1% FA; flow rate: 300 nL/min over 30 min and 5 min to 55%). The LTQ-Orbitrap Velos was operated in the positive ion mode applying a data-dependent automatic switch between survey mass spectra (MS) scan and tandem mass spectra (MS/MS) acquisition. MS scans were acquired in the mass range of m/z 400 to 1400 with 30,000 resolution at m/z 400, with lock mass option enabled for the 445.120025 ion [200]. The 10 most intense peaks having ≥2 charge state and above 500 intensity threshold were selected for fragmentation by high energy collision-induced dissociation (HCD) at 42% normalized energy, 100 ms activation time and 2 m/z precursor isolation width. Maximum injection time was 1,000 ms and 500 ms for survey and MS/MS scans, respectively. Automatic gain control was 1

$\times 10^6$ for MS and 5×10^4 for MS/MS scans. Dynamic exclusion was enabled for 90 s. MS/MS spectra were acquired in the Orbitrap with 7,500 resolution. A parent mass list with m/z corresponding to possible acetylated peptides was build using Skyline and included in the acquisition method [201].

Mass spectra were analyzed using the SEQUEST HT algorithm of the Proteome Discoverer software (Cat. #OPTON-30795, Thermo Fisher Scientific). All tandem mass spectra were searched against a custom database containing Uniprot complete mouse sequences and Mann contaminants. The search parameters were fully-tryptic digestion with a maximum of 2 missed cleavages, 20 ppm and 0.02 Da mass tolerances for precursor and product ions respectively, carbamidomethylated cysteines, variable oxidation of methionine and variable acetylation on lysine. 1% false discovery rate using Percolator [199] was used for peptide validation. In order to evaluate the proportion of acetylated peptides, a mass deviation of 2 ppm was used for precursor ion area detection, and peptides with 5% false discovery rate were also included in the calculation. Spectra of peptides identified as acetylated were manually inspected for the presence of acetylation marker ions [201, 202].

1.18 Image processing

All images and figures were assembled and processed for final presentation with Canvas Draw 2 for Mac software (version 2.0, Canvas X).

1.19 Statistical analyses

Statistical analyses were carried out using GraphPad Prism software (version 6.0 and 8.0). The number of replicates and the statistical test used in each case are indicated in the figure legends. In all cases, the *P* values have been depicted using the * (when < 0.05), ** (when < 0.01), and *** (when < 0.001) notation.

2. METHODS USED IN CHAPTER 3

2.1 Animals

Vav2$^{Onc/Onc}$ (C57BL/6 background) and *Vav2*$^{-/-}$ (C57BL/10 genetic background) mice have been described before [83, 102]. *Vav2*$^{L332A/L332A}$ knock-in mice (mixed genetic background, generated by GenOway, Lyon, France) will be described elsewhere (L.F.L-M., S.R-F. and X.R.B., manuscript submitted). All mice and their proper WT controls were housed with an artificial 12-hour light /12-hour dark cycle under controlled temperature and humidity conditions. They were routinely maintained under ad libitum access to a standard chow global diet (Cat. #2018; Teklad global 18% protein) and tap water. When indicated, 8-week-old mice were shifted to a HFD (45% fat, 4.73 kcal/g; Cat. #D12451; Research Diets) for four months before being euthanized. All the experiments were performed according to protocols approved by the Bioethics Committees of both the University of Salamanca and the University of Santiago de Compostela.

2.2 Cell lines

C2C12 cells were obtained from P. Muñoz-Cánovas (University Pompeu-Fabra, Barcelona, Spain) and cultured in DMEM containing 10% fetal bovine serum, 1% L-glutamine, penicillin (10 µg/ml) and streptomycin (100 µg/mL) and maintained at 37 ºC and a 5% CO_2 humidified atmosphere. All the reagents were obtained from Gibco. For cell stimulation studies, C2C12 cells were starved for 3 hours and then stimulated with insulin (75 nM; CN #775502, Actrapid NovoNordisk) for the indicated times. When indicated, cells were treated for 1 hour with the indicated concentration of Wortmannin (Cat. #19545-26-7, Calbiochem), PIK-75 (Cat. #372196-77-5, Cayman Chemical) or TGX-221 (Cat. #663619-89-4, Cayman Chemical). The Lenti-X 293T lentiviral packaging cell line was obtained from Clontech (Cat. #632180) and cultured as above.

2.3 Mammalian expression vectors

All the constructs used in this work encode the murine versions of the proteins and were DNA sequence-verified in our Genomics facility. Plasmids encoding EGFP-Vav2 (pAA7) and EGFP-Rac1^{Q61L} (pNM42) have already been described [190, 203]. To generate the plasmid encoding EGFP-Vav2^{Onc} (pNM115), the plasmid pKES19 [23] was

digested with BstXI, filled-in, and cloned into the SmaI-linearized pEGFP-C2 vector (Clontech, Cat. #632481). The plasmid encoding EGFP-Vav2$^{Onc+E200A}$ (pFLM07) was obtained by site-directed mutagenesis using the plasmid pNM115 as template for the PCR, the high-fidelity Pfu Turbo DNA polymerase (Cat. #600250, Agilent), and the primers 5'-GAC AAG AGA AGC TGC TGC TTG TTA GCG ATT CAG GAG ACC GAG GCC AAG TAC-3' and 5'-CAT GAA CCG GAG CCA GAG GAC TTA GCG ATT GTT CGT CGT CGA AGA GAA CAG-3' (the altered nucleotides used to create the E200A mutation are underlined). The plasmids pMD-G and pNGVL-MLV-gag-pol were provided by Drs. R.C. Mulligan (Children's Hospital, Boston, MA, USA) and A. Bernard (CNIC, Madrid, Spain, EU), respectively. The pEGFP-C1-PH-Akt and pmCherry-C1-PH-Akt vectors were obtained from Dr. J.P. Simas (Lisbon University, Lisbon, Portugal) [204].

To generate the lentiviral vector encoding HA-tagged Vav2^{Onc} (pCCM34), a cDNA fragment encoding HA-Vav2^{Onc} was amplified by PCR using the plasmid pCMV-Vav2 HA as template[204] and the primers 5'-AAT AAC TAG TGC CAC CAT GTA CCC ATA CGA CGT CCC AGA CTA CGC TAA AAT GGG AAT GAC TGA GGA CGA C-3' and 5'-ATA GAC CGC GGC CGC TCA CTG GAT GCC CTC CTC TTC TAC GTA-3' (restriction sites underlined). Upon purification and digestion with SpeI and NotI, the fragment was cloned into the SpeI-NotI linearized pLVX-IRES-Hyg vector (Cat. #632185, Clontech). The pCCM34 vector was used as template to generate the plasmid encoding HA-Vav2$^{Onc+E200A}$ (pFLM12) by site-directed mutagenesis using the primers 5'- GAC AAG AGA AGC TGC TGC TTG TTA GCG ATT CAG GAG ACC GAG GCC AAG TAC -3' and 5'-CAT GAA CCG GAG CCA GAG GAC TTA GCG ATT GTT CGT CGT CGA AGA GAA CAG -3' to introduce the mutation E200A (the altered nucleotides used to create the E200A mutation are underlined). Site-directed mutagenesis was performed using the high–fidelity NZYProof DNA polymerase (Cat. #14601, NZYTech).

2.4 Nuclear magnetic resonance

Body composition was measured by nuclear magnetic resonance (Whole Body Composition Analyzer; EchoMRI, Houston, TX) as indicated [205].

2.5 Histology

Tissues were extracted, fixed in 4% paraformaldehyde (Cat. #252931, PanReac), paraffin embedded, cut in 2–3 µm (in the case of muscle, liver and BAT) or 5 µm (in the case of the WAT) thick sections, and stained with hematoxylin-eosin. Images were captured using an Olympus BX51 microscope coupled to an Olympus DP70 digital camera.

2.6 Histological quantifications

The cross-sectional area of the skeletal fibers was measured with the ImageJ software (National Institutes of Health, Bethesda, MD) using the Region of Interest Manager tool and manually selecting the limits of at least 50 fibers per animal. Two independent regions of hematoxylin-eosin-stained gastrocnemius sections (x400 amplified pictures) were used for each quantification. Values obtained were transformed according to the scale used.

The diameter of the adipocytes was measured using x100 amplified images of the stained histology samples from either 2 or 3 representative regions per animal utilizing the macro "Adipocyte Tool" of the ImageJ software [206]. To this end, the options in the "p" and "s" buttons of macro were configured for values between 80 and 20 000 using the Huang thresholding method. Errors in the automatic detection of the adipocytes were manually corrected. Values obtained were transformed according to the scale used.

The number of nuclei per field in BAT was quantified in hematoxylin-eosin-stained sections with ImageJ using at least two different x200 amplified pictures per animal. After splitting the color channels, the threshold was adjusted in the red channel to select the cell nuclei. The number of nuclei was obtained using the tool "Analyze Particles" after the selection of the adequate size range. For the analysis of the brown adipose tissue lipid vacuoles, the green channel was selected after the color separation and the colors inverted to visualize the vacuoles in black. The threshold was adjusted to select the lipid droplets. The size of the vacuoles was quantified using also the ImageJ "Analyze Particles" tool.

2.7 Isolation of muscle satellite cells

Muscles were minced with razors and digested twice in DMEM media containing collagenase D (0.08%, Cat. # 11088866001; Roche) and trypsin (0.125%, Cat. #1590-

046; Invitrogen) at 37 ºC for 25 min in a shaking water bath. Samples were then centrifuged at low speed and the digestion repeated with the pelleted fragments. Cells were then filtered, centrifuged, and incubated in Lysis buffer 1x (Cat. #555899; BD) for 10 min on ice. After centrifugation, cells were resuspended in phosphate-buffered saline solution supplemented with 2.5% fetal bovine serum (Cat. #10270, Gibco) and stained for 20 min with allophycocyanine-conjugated anti-CD45 (Cat# 103112, BioLegend), Pacific blue-conjugated-conjugated Sca1 (Cat. #108119, BioLegend), phycoerythrin-conjugated-conjugated anti-α7-integrin (Cat# 53-0010-05, Ablab), and fluorescein isothiocyanate-conjugated-conjugated anti-CD34 (Cat. #11-0341-82, eBioscience). $Sca1^{-}$;$CD45^{-}$;integrin $\alpha7^{+}$;$CD34^{+}$ cells were sorted using a FACS Aria II (BD). The purified satellite cells were cultured in Ham's F10 medium (Cat. #11550-043, Gibco) supplemented with 30% fetal bovine serum (Cat. #10270, Gibco) and 0.025 µg/ml human basic fibroblast growth factor (Cat. #hFGDBCF, Immunostep) on collagen type I-coated wells (Cat. #3447-020-01, Cultrex, R&D systems).

2.8 In vitro activation and proliferation of satellite cells

1000 cells were plated on collagen I-treated 10 mm diameter coverslips in 12-well plates with growth medium. After 24 (before the first division to assess activation) and 72 (to assess proliferation) hours in culture, cells were labeled with EdU (Click-iT EdU Alexa Fluor 647 Imaging kit, Cat. #C10340; Invitrogen) according to the manufacturer's instructions and stained with 4',6-diamidino-2-phenylindole dihydrochloride (1 µg/mL, Cat. #D1306; Invitrogen). The percentage of EdU positive cells was quantified under a fluorescence microscope.

2.9 Myogenic differentiation of satellite and C2C12 cells

10 000 satellite cells were plated on collagen I-treated 12-well plates and maintained in Ham's F10 medium supplemented with 30% fetal bovine serum and 0.025 µg/ml human basic fibroblast growth factor until a 70 % confluence was reached. The fetal bovine serum in the medium was then decreased to a 2% and replaced every other day until the end of the experiment. C2C12 cells were shifted into a differentiation medium (DMEM supplemented with 2% horse serum (Cat. #16050122, Gibco), 1% L-glutamine, penicillin

(10 µg/ml) and streptomycin (100 µg/ml) when they reached 80% confluency. Medium was replaced since then every other day until the end of the experiment.

2.10 Immunofluorescence

Cells were fixed in 4% formaldehyde (Cat. #F8775, Sigma) in phosphate-buffered saline solution for 30 min, washed twice with phosphate-buffered saline solution, permeabilized with 0.5% Triton X–100 (Cat. #X100, Sigma) in TBS-T [25 mM Tris–HCl (pH 8.0), 150 mM NaCl, 0.1 % Tween–20 (Cat. #P7949, Sigma)] for 15 min, washed three times with TBS–T, blocked in TBS–T supplemented with 2 % bovine serum albumin (Cat. #A4503, Sigma) for 2 hours, and then incubated with antibodies to MHCII (1:700, Cat. #M4276; Sigma) in blocking buffer at 4 °C overnight. Alexa Fluor 647-labeled goat anti-mouse IgG (1:500 in blocking buffer, Cat. #A28181; Thermo Fisher Scientific) was used as secondary antibody. After 30 min, the cells were washed three times in TBS-T and, finally, stained with 1 µg/mL of 4',6–diamidino–2–phenylindole (Cat. #D1306, Invitrogen) for 5 min to visualize the nuclei. Images were captured in an EVOS FL Cell Imaging System microscope (Cat. #AMF4300, Thermo Fisher Scientific).

2.11 RNA isolation and quantitation

Total RNA was isolated using NZYol (Cat. # MB18501, NZYtech) and analyzed by qRT-PCR using the Power SYBR Green RNA-to-CT™ 1-Step Kit (Cat. #4389986, Applied Biosystems) and the StepOnePlus Real-Time PCR System (Cat. #4376600, Applied BioSystems) according to the supplier's instructions. Raw qRT-PCR data were processed with the StepOne software v2.1 (Applied Biosystems) using *Gadph* as intersample normalization control. Primers used included 5'-AGT CCC AGG TCA ACA AGC TG-3' (forward for *Myh1* and *Myh4*), 5'-TCT TTG GTC ACT TTC CTG CAC T-3' (reverse for *Myh1*), 5'-TTT CTC CTG TCA CCT CTC AAC A-3' (reverse for *Myh4*), 5'-CAC TGG AGT TCG GTC CCA A-3' (forward for *MyoG*), 5'-TGT GGG CGT TAG GGT C-3' (reverse for *MyoG*), 5'-GTG AAT GAG ATG GCG AGG GT-3' (forward for *Hsl*), 5'-GAG CTC CGC CTT TAA TGG GT-3' (reverse for *Hsl*), 5'-GTC GGT CCT TCC TTG GTG TA-3' (forward for *Ucp1*), 5'-TGC ACC ACC AAC TGC TTA GC-3' (reverse for *Ucp1*), 5'-GAG GGG CTA CCT TCC TCT CA-3' (forward for *Trim63*), 5'-

TTT ACC CTC TGT GGT CAC GC-3' (reverse for *Trim63*), 5'-TCT GGG ACC TTA GGA GAG CC-3' (forward for *Fbxo32*), 5'-CCC CCA CCC CAG GAA TTA AC-3' (reverse for *Fbxo32*), 5'-TGC ACC ACC AAC TGC TTA GC-3' (forward for *Gapdh*), 5'-TCT TCT GGG TGG CAG TGA TG-3' (reverse for *Gapdh*).

2.12 In vivo infusion of mice with insulin and IGF-1

Mice were fasted for 7 hours, deeply anesthetized with a combination of ketamine (CN #571267.3; Merial) plus xylazine (Cat. #572126.2; Bayer), and injected via the inferior vena cava with either insulin (0.5 UI/kg, Cat. #775502; Actrapid NovoNordisk) or IGF-1 (0.2 and 0.5 mg/kg in the case of *Vav2*$^{Onc/Onc}$ and *Vav2*$^{L332A/L332A}$ mice, respectively; Cat. #100-11, PreproTech). After 2 (liver), 5 (skeletal muscle) and 7 (perigonadal WAT) min, tissues were collected and snap frozen.

2.13 Western blotting

In the case of mouse tissue extracts, the frozen samples were disrupted with the help of a Dispomix Drive homogenizer (Cat. #900020.00, Medic Tools AG) in gentleMACS M tubes (Cat. # 130-096-335, Myltenyi Biotec) in ice-cold lysis buffer [50 mM Tris-HCl (pH 7.5), 1 mM ethylene glycol tetraacetic acid (Cat. #E3889, Sigma), 1 mM ethylenediaminetetraacetic acid (Cat. #ED-2SS, Sigma), 1% Triton X-100 (Cat. #X100, Sigma), 1 mM sodium orthovanadate (Cat. #S6508, Sigma), 50 mM sodium fluoride (Cat. #S7920, Sigma), 5 mM sodium pyrophosphate (Cat. #221368; Sigma), 0.27 M sucrose (Cat. #S9378, Sigma), 1 mM phenylmethanesulfonyl fluoride (Cat. #P7626, Sigma) and cØmplete Protease Inhibitor Cocktail (Cat. #11836145001, Roche)]. After a short centrifugation to eliminate cellular debri, the samples were centrifuged once (in the case of muscle), twice (in the case of liver) or thrice (in the case of WAT) at 4 ºC and 10 000 rpm for 30 min to clarify the sample. In the case of extracts from cultured cells, samples were washed with phosphate-buffered saline solution and lysed in RIPA buffer [10 mM Tris-HCl (pH 7.5), 150 mM sodium chloride, 1% Triton X-100 (Cat. #X100, Sigma), 1 mM sodium orthovanadate (Cat. #S6508, Sigma), 1 mM sodium fluoride (Cat. #S7920; Sigma) and CØmplete Protease Inhibitor Cocktail]. Cellular extracts were kept 5 min on ice and centrifuged at 14 000 rpm for 10 min at 4 ºC. Regardless of the source, protein extracts were separated electrophoretically in SDS-PAGE gels, transferred onto nitrocellulose membranes, and subjected to immunoblot analyses as described in the first

part of the methods section. Antibodies used include those to phospho-Akt (Thr^{308}) (dilution 1:1000; Cat. #4056, Cell Signaling Technologies), Akt (dilution 1:1000; Cat. #2920, Cell Signaling Technologies), phospho-GSK3α/β (dilution 1:1000; Cat. #9327, Cell Signaling Technologies), GSK3α/β (dilution 1:1000; Cat. #5676, Cell Signaling Technologies), phospho-S6K (Thr^{389}) (dilution 1:1000; Cat. #9215, Cell Signaling Technologies), tubulin α (dilution 1:2000; Cat. #CP06, Calbiochem), MHCII (dilution 1:2000; Cat. #M4276; Sigma), S6K (dilution 1:1000; Cat. #sc-7020, Santa Cruz Biotechnology), and HA (dilution 1:1000; Cat. #3724, Cell Signaling Technologies). The polyclonal rabbit antibody to Vav2 (dilution 1:1000) was homemade using as epitope the acidic region of this protein [101]. For quantification of the relative protein phosphorylation levels, the intensity of the bands was measured with the ImageJ software. Values were normalized taken into consideration the amount of total protein present in each sample.

2.14 Generation of stable cell lines

We used the CRISPR/Cas9-gene editing strategy to knockout the *Vav2* locus in C2C12 cells. To this end, two different sgRNAs targeting the exon 1 of *Vav2* at the sequences 5'-CGC CCA ACC ACC GCG TCG TG-3' (guide 1) and 5'-GCA GTG CCG GGA CCC TCA CC-3' (guide 2) were annealed and ligated into the plasmid pSpCas9(BB)-2A-GFP (Cat. #48138, Addgene). Plasmids were introduced into C2C12 cells using Lipofectamine 2000 (Cat. #11668019; Invitrogen) and, 36 hours later, the GFP positive cells were single-cell sorted using a FACS Aria II (BD) to obtain individual clones. Cell clones were grown in 96 well plates, screened by PCR, and further verified by both DNA sequencing and immunoprecipitation. To this end, 2 mg of protein extracts obtained from C2C12 cells were incubated in 1 mL of RIPA buffer with 1.5 µL of antibody to Vav2 (see above) for 2 hours at 4ºC. Immunocomplexes were collected with Gammabind G-Sepharose beads (Cat. # GE17-0885-01; GE Healthcare), washed three times in RIPA buffer, resuspended in SDS-PAGE buffer, boiled for 5 min, and subjected to immunoblot analysis using antibodies to Vasv2 as indicated above. Independent clones (WT and *Vav2* null) were then used in the experiments.

Cell pools ectopically expressing the indicated proteins were generated using a lentiviral delivery method. To generate the viral particles, 2.5 µg of pMD-G, 7.5 µg of pNGVL-MLV-gag-pol, and 10 µg of the appropriate lentiviral plasmid were transfected

into HEK293T cells using Lipofectamine 2000 according to the manufacturer's instructions. Cell culture supernatants were collected 24, 48 and 72 hours later, passed through 0.45 μm filters (Cat. #10462100, GE Healthcare), supplemented with Polybrene (8 μg/ml; Cat. #H9268, Sigma) and poured onto exponentially growing C2C12 cells. 24 hours after the infection, the cells were washed and selected with hygromycin B (Cat. #21414000, Roche). Expression of proteins was verified using immunoblots with antibodies to the HA epitope.

2.15 In vivo detection of PI3K activation using bioreporters

1 x 10^6 exponentially growing C2C12 cells were electroporated using the Neon Transfection System (1650 V, 15 msec, 2 pulses; Cat. #MPK5000, Invitrogen) and 20 μg of the appropriate plasmids following the manufacturer's instructions. In all cases, cells were transfected with the bioreporter-encoding plasmid (pEGFP-C1-PH-Akt or pmCherry-C1-PH-Akt) and, whenever required, cotransfected with expression vectors expressing the indicated EGFPs. After 36 hours, cells were trypsinized, resuspended in serum-free medium, and replated onto coverslips. After 3 hours of starvation plus the indicated treatments, cells were either left stimulated or stimulated with 75 nM insulin for 10 min. Cells were then washed with phosphate-buffered saline solution, fixed in 4% formaldehyde (Cat. #F8775, Sigma) in phosphate-buffered saline solution for 15 min, permeabilized in 0.5% Triton X-100 in TBS-T for 10 min, washed in phosphate–buffered saline solution, and mounted with Mowiol (Cat. #475904, Calbiochem). Images were captured with LAS AF software (version 2.6.0.72266, Leica) in a Leica TCS SP5 confocal microscope.

2.16 Glucose and insulin tolerance tests

The animals were fasted overnight for 14 hours and basal blood glucose levels measured with an Accu–Chek glucometer using blood samples collected from tail bleeds (Cat. #04680430003, Roche). In the case of glucose and insulin tolerance test, mice fasted as above were injected intraperitoneally with either D-glucose (2 g/kg; Cat. #G8270, Sigma) or insulin (0.5 units/kg; CN #775502, Actrapid NovoNordisk). The levels of glucose in plasma were determined from tail bleeds taken at the indicated time-points.

2.17 Determination of plasma concentrations of insulin and C-peptide

Levels of insulin and C-peptide were determined in blood samples using the Rat/Mouse Insulin (Cat. #EZRMI-13K, Merck Millipore) and the mouse C-peptide (Cat. #80-CPTMS-E01, Alpco) ELISA kits, respectively.

2.18 Determination of triglyceride concentration in liver

Liver fragments (50 mg) were manually homogenized by mincing with a scalpel blade and triglycerides extracted in 500 µL of an ice-cold chloroform-methanol solution (2:1, vol/vol) by shaking in a thermoblock at room temperature for 2 hours. For phase separation, Milli-Q water (Millipore) was added and samples centrifuged at room temperature for 30 minutes at 10 000 rpm. The organic bottom layers resulting from that centrifugation were collected in a new tube, dried up using a vacuum concentrator centrifuge (UNI VAPO 100 ECH; UniEquip) and resuspended in chloroform. After evaporation of the organic solvent in a thermoblock, the solid residue was resuspended in the Triglycerides-LQ reagent (Cat. #1001314, Spinreact) and triglyceride content determined using a spectrophotometer (Cat. #170-2501, BioRad).

2.19 Metabolic determinations

Food intake of individually–caged mice was measured every other day. Energy expenditure, respiratory quotients, and locomotor activity of animals were analyzed using a calorimetric system (LabMaster, TSE Systems, Bad Homburg, Germany). Rectal temperature was measured using a digital thermometer (VedoBEEP, Artsana, Grandate, Italy). Skin temperature surrounding BAT was recorded with an infrared camera (B335:Compact-Infrared-Thermal-Imaging-Camera, FLIR, West Malling, Kent, UK) as previously described [96].

2.20 Statistical analyses

The number of replicates (n), the type of statistical test performed, and the statistical significance for each experiment is indicated in the appropriate figure legend. Whenever possible, data normality was analyzed using Shapiro–Wilk tests. Nonparametric tests were applied to non-normally distributed data. In the case of Student's *t* tests,

REFERENCES

1. Hall, A. (1998). Rho GTPases and the actin cytoskeleton. Science *279*, 509-514.

2. Etienne-Manneville, S., and Hall, A. (2002). Rho GTPases in cell biology. Nature *420*, 629-635.

3. Heasman, S.J., and Ridley, A.J. (2008). Mammalian Rho GTPases: new insights into their functions from in vivo studies. Nat Rev Mol Cell Biol *9*, 690-701.

4. Croise, P., Estay-Ahumada, C., Gasman, S., and Ory, S. (2014). Rho GTPases, phosphoinositides, and actin: a tripartite framework for efficient vesicular trafficking. Small GTPases *5*, e29469.

5. Wojnacki, J., Quassollo, G., Marzolo, M.P., and Caceres, A. (2014). Rho GTPases at the crossroad of signaling networks in mammals: impact of Rho-GTPases on microtubule organization and dynamics. Small GTPases *5*, e28430.

6. Ridley, A.J. (2015). Rho GTPase signalling in cell migration. Curr Opin Cell Biol *36*, 103-112.

7. Lawson, C.D., and Ridley, A.J. (2018). Rho GTPase signaling complexes in cell migration and invasion. J Cell Biol *217*, 447-457.

8. Rossman, K.L., Der, C.J., and Sondek, J. (2005). GEF means go: turning on RHO GTPases with guanine nucleotide-exchange factors. Nat Rev Mol Cell Biol *6*, 167-180.

9. Cook, D.R., Rossman, K.L., and Der, C.J. (2014). Rho guanine nucleotide exchange factors: regulators of Rho GTPase activity in development and disease. Oncogene *33*, 4021-4035.

10. Hodge, R.G., and Ridley, A.J. (2016). Regulating Rho GTPases and their regulators. Nat Rev Mol Cell Biol *17*, 496-510.

11. Movilla, N., Dosil, M., Zheng, Y., and Bustelo, X.R. (2001). How Vav proteins discriminate the GTPases Rac1 and Rhoa from Cdc42. Oncogene *20*, 8057-8065.

12. Bustelo, X.R. (2014). Vav family exchange factors: an integrated regulatory and functional view. Small GTPases *5*, 9.

13. Sebe-Pedros, A., Burkhardt, P., Sanchez-Pons, N., Fairclough, S.R., Lang, B.F., King, N., and Ruiz-Trillo, I. (2013). Insights into the origin of metazoan filopodia and microvilli. Mol Biol Evol *30*, 2013-2023.

14. Manning, G., Young, S.L., Miller, W.T., and Zhai, Y. (2008). The protist, Monosiga brevicollis, has a tyrosine kinase signaling network more elaborate and

diverse than found in any known metazoan. Proc Natl Acad Sci U S A *105*, 9674-9679.

15. Brunet, T., and King, N. (2017). The Origin of Animal Multicellularity and Cell Differentiation. Dev Cell *43*, 124-140.

16. Flajnik, M.F., and Kasahara, M. (2010). Origin and evolution of the adaptive immune system: Genetic events and selective pressures. In Nature Reviews Genetics.

17. Rodriguez-Fdez, S., and Bustelo, X.R. (2019). The Vav GEF Family: An Evolutionary and Functional Perspective. Cells *8*.

18. Wu, J., Katzav, S., and Weiss, A. (1995). A functional T-cell receptor signaling pathway is required for p95vav activity. Mol Cell Biol *15*, 4337-4346.

19. Zhou, Z., Yin, J., Dou, Z., Tang, J., Zhang, C., and Cao, Y. (2007). The calponin homology domain of Vav1 associates with calmodulin and is prerequisite to T cell antigen receptor-induced calcium release in Jurkat T lymphocytes. J Biol Chem *282*, 23737-23744.

20. Robles-Valero, J., Lorenzo-Martin, L.F., Menacho-Marquez, M., Fernandez-Pisonero, I., Abad, A., Camos, M., Toribio, M.L., Espinosa, L., Bigas, A., and Bustelo, X.R. (2017). A Paradoxical Tumor-Suppressor Role for the Rac1 Exchange Factor Vav1 in T Cell Acute Lymphoblastic Leukemia. Cancer Cell *32*, 608-623 e609.

21. Barreira, M., Fabbiano, S., Couceiro, J.R., Torreira, E., Martinez-Torrecuadrada, J.L., Montoya, G., Llorca, O., and Bustelo, X.R. (2014). The C-terminal SH3 domain contributes to the intramolecular inhibition of Vav family proteins. Sci Signal *7*, ra35.

22. Crespo, P., Schuebel, K.E., Ostrom, A.A., Gutkind, J.S., and Bustelo, X.R. (1997). Phosphotyrosine-dependent activation of Rac-1 GDP/GTP exchange by the vav proto-oncogene product. Nature *385*, 169-172.

23. Schuebel, K.E., Movilla, N., Rosa, J.L., and Bustelo, X.R. (1998). Phosphorylation-dependent and constitutive activation of Rho proteins by wild-type and oncogenic Vav-2. EMBO J *17*, 6608-6621.

24. Yu, B., Martins, I.R.S., Li, P., Amarasinghe, G.K., Umetani, J., Fernandez-Zapico, M.E., Billadeau, D.D., Machius, M., Tomchick, D.R., and Rosen, M.K. (2010). Structural and Energetic Mechanisms of Cooperative Autoinhibition and Activation of Vav1. Cell *140*, 246-256.

25. Couceiro, J.R., Martin-Bermudo, M.D., and Bustelo, X.R. (2005). Phylogenetic conservation of the regulatory and functional properties of the Vav oncoprotein family. Exp Cell Res *308*, 364-380.

26. Norman, K.R., Fazzio, R.T., Mellem, J.E., Espelt, M.V., Strange, K., Beckerle, M.C., and Maricq, A.V. (2005). The Rho/Rac-Family guanine nucleotide exchange factor VAV-1 regulates rhythmic behaviors in C. elegans. Cell *123*, 119-132.

27. Movilla, N., and Bustelo, X.R. (1999). Biological and regulatory properties of Vav-3, a new member of the Vav family of oncoproteins. Mol Cell Biol *19*, 7870-7885.

28. Zugaza, J.L., Lopez-Lago, M.A., Caloca, M.J., Dosil, M., Movilla, N., and Bustelo, X.R. (2002). Structural determinants for the biological activity of Vav proteins. J Biol Chem *277*, 45377-45392.

29. Aghazadeh, B., Lowry, W.E., Huang, X.Y., and Rosen, M.K. (2000). Structural basis for relief of autoinhibition of the Dbl homology domain of proto-oncogene Vav by tyrosine phosphorylation. Cell *102*, 625-633.

30. Lopez-Lago, M., Lee, H., Cruz, C., Movilla, N., and Bustelo, X.R. (2000). Tyrosine phosphorylation mediates both activation and downmodulation of the biological activity of Vav. Mol Cell Biol *20*, 1678-1691.

31. Barreira, M., Rodríguez-Fdez, S., and Bustelo, X.R. (2018). New insights into the Vav1 activation cycle in lymphocytes. Cell Signal *45*, 132-144.

32. Bustelo, X.R., Ledbetter, J.A., and Barbacid, M. (1992). Product of vav proto-oncogene defines a new class of tyrosine protein kinase substrates. Nature *356*, 68-71.

33. Margolis, B., Hu, P., Katzav, S., Li, W., Oliver, J.M., Ullrich, A., Weiss, A., and Schlessinger, J. (1992). Tyrosine phosphorylation of vav proto-oncogene product containing SH2 domain and transcription factor motifs. Nature *356*, 71-74.

34. Weng, W.K., Jarvis, L., and LeBien, T.W. (1994). Signaling through CD19 activates Vav/mitogen-activated protein kinase pathway and induces formation of a CD19/Vav/phosphatidylinositol 3-kinase complex in human B cell precursors. J Biol Chem *269*, 32514-32521.

35. O'Rourke, L.M., Tooze, R., Turner, M., Sandoval, D.M., Carter, R.H., Tybulewicz, V.L., and Fearon, D.T. (1998). CD19 as a membrane-anchored adaptor protein of B lymphocytes: costimulation of lipid and protein kinases by recruitment of Vav. Immunity *8*, 635-645.

36. Doody, G.M., Billadeau, D.D., Clayton, E., Hutchings, A., Berland, R., McAdam, S., Leibson, P.J., and Turner, M. (2000). Vav-2 controls NFAT-dependent transcription in B- but not T-lymphocytes. EMBO J *19*, 6173-6184.

37. Son, M., Park, I., Lee, O.H., Rhee, I., Park, C., and Yun, Y. (2012). LIME mediates immunological synapse formation through activation of VAV. Molecules and cells *33*, 407-414.

38. Johmura, S., Oh-hora, M., Inabe, K., Nishikawa, Y., Hayashi, K., Vigorito, E., Kitamura, D., Turner, M., Shingu, K., Hikida, M., *et al.* (2003). Regulation of Vav localization in membrane rafts by adaptor molecules Grb2 and BLNK. Immunity *18*, 777-787.

39. Wu, J., Motto, D.G., Koretzky, G.A., and Weiss, A. (1996). Vav and SLP-76 interact and functionally cooperate in IL-2 gene activation. Immunity *4*, 593-602.

40. Tuosto, L., Michel, F., and Acuto, O. (1996). p95vav associates with tyrosine-phosphorylated SLP-76 in antigen-stimulated T cells. J Exp Med *184*, 1161-1166.

41. Lindholm, C.K., Henriksson, M.L., Hallberg, B., and Welsh, M. (2002). Shb links SLP-76 and Vav with the CD3 complex in Jurkat T cells. Eur J Biochem *269*, 3279-3288.

42. Pauker, M.H., Hassan, N., Noy, E., Reicher, B., and Barda-Saad, M. (2012). Studying the dynamics of SLP-76, Nck, and Vav1 multimolecular complex formation in live human cells with triple-color FRET. Sci Signal *5*, rs3.

43. Barda-Saad, M., Shirasu, N., Pauker, M.H., Hassan, N., Perl, O., Balbo, A., Yamaguchi, H., Houtman, J.C., Appella, E., Schuck, P., *et al.* (2010). Cooperative interactions at the SLP-76 complex are critical for actin polymerization. EMBO J *29*, 2315-2328.

44. Gomez, T.S., Hamann, M.J., McCarney, S., Savoy, D.N., Lubking, C.M., Heldebrant, M.P., Labno, C.M., McKean, D.J., McNiven, M.A., Burkhardt, J.K., *et al.* (2005). Dynamin 2 regulates T cell activation by controlling actin polymerization at the immunological synapse. Nat Immunol *6*, 261-270.

45. Sylvain, N.R., Nguyen, K., and Bunnell, S.C. (2011). Vav1-mediated scaffolding interactions stabilize SLP-76 microclusters and contribute to antigen-dependent T cell responses. Sci Signal *4*, ra14.

46. Charvet, C., Canonigo, A.J., Billadeau, D.D., and Altman, A. (2005). Membrane localization and function of Vav3 in T cells depend on its association with the adapter SLP-76. J Biol Chem *280*, 15289-15299.

47. Aoki, K. (2005). Local Phosphatidylinositol 3,4,5-Trisphosphate Accumulation Recruits Vav2 and Vav3 to Activate Rac1/Cdc42 and Initiate Neurite Outgrowth in Nerve Growth Factor-stimulated PC12 Cells. Mol Biol Cell *16*, 2207-2217.

48. Arudchandran, R., Brown, M.J., Peirce, M.J., Song, J.S., Zhang, J., Siraganian, R.P., Blank, U., and Rivera, J. (2000). The Src homology 2 domain of Vav is required for its compartmentation to the plasma membrane and activation of c-Jun NH(2)-terminal kinase 1. J Exp Med *191*, 47-60.

49. Bartolomé, R.A., Molina-Ortiz, I., Samaniego, R., Sánchez-Mateos, P., Bustelo, X.R., and Teixidó, J. (2006). Activation of Vav/Rho GTPase signaling by CXCL12 controls membrane-type matrix metalloproteinase-dependent melanoma cell invasion. Cancer Research *66*, 248-258.

50. Houlard, M., Arudchandran, R., Regnier-Ricard, F., Germani, A., Gisselbrecht, S., Blank, U., Rivera, J., and Varin-Blank, N. (2002). Vav1 Is a Component of Transcriptionally Active Complexes. J Exp Med *195*, 1115-1127.

51. Blanchet, F., Cardona, A., Letimier, F.A., Hershfield, M.S., and Acuto, O. (2005). CD28 costimulatory signal induces protein arginine methylation in T cells. J Exp Med *202*, 371-377.

52. Ward, S.G., Ley, S.C., Macphee, C., and Cantrell, D.A. (1992). Regulation of D-3 phosphoinositides during T cell activation via the T cell antigen receptor/CD3 complex and CD2 antigens. Eur J Immunol *22*, 45-49.

53. Gulbins, E., Coggeshall, K.M., Baier, G., Telford, D., Langlet, C., Baier-Bitterlich, G., Bonnefoy-Berard, N., Burn, P., Wittinghofer, A., and Altman, A. (1994). Direct stimulation of Vav guanine nucleotide exchange activity for Ras by phorbol esters and diglycerides. Mol Cell Biol *14*, 4749-4758.

54. Kazanietz, M.G., Bustelo, X.R., Barbacid, M., Kolch, W., Mischak, H., Wong, G., Pettit, G.R., Bruns, J.D., and Blumberg, P.M. (1994). Zinc finger domains and phorbol ester pharmacophore. Analysis of binding to mutated form of protein kinase C ζ and the vav and c-raf proto-oncogene products. J Biol Chem *269*, 11590-11594.

55. Park, W.S., Do Heo, W., Whalen, J.H., O'Rourke, N.A., Bryan, H.M., Meyer, T., and Teruel, M.N. (2008). Comprehensive Identification of PIP3-Regulated PH Domains from C. elegans to H. sapiens by Model Prediction and Live Imaging. Mol Cell *30*, 381-392.

56. Geczy, T., Peach, M.L., Kazzouli, S.E., Sigano, D.M., Kang, J.H., Valle, C.J., Selezneva, J., Woo, W., Kedei, N., Lewin, N.E., *et al.* (2012). Molecular basis for failure of "atypical" C1 domain of Vav1 to bind diacylglycerol/phorbol ester. J Biol Chem *287*, 13137-13158.

57. Inabe, K., Ishiai, M., Scharenberg, A.M., Freshney, N., Downward, J., and Kurosaki, T. (2002). Vav3 Modulates B Cell Receptor Responses by Regulating Phosphoinositide 3-Kinase Activation. J Exp Med *195*, 189-200.

58. Reynolds, L.F., Smyth, L.A., Norton, T., Freshney, N., Downward, J., Kioussis, D., and Tybulewicz, V.L. (2002). Vav1 transduces T cell receptor signals to the activation of phospholipase C-gamma1 via phosphoinositide 3-kinase-dependent and -independent pathways. J Exp Med *195*, 1103-1114.

59. Vigorito, E., Bardi, G., Glassford, J., Lam, E.W.-F., Clayton, E., and Turner, M. (2004). Vav-Dependent and Vav-Independent Phosphatidylinositol 3-Kinase Activation in Murine B Cells Determined by the Nature of the Stimulus. J Immunol *173*, 3209-3214.

60. Pires De Miranda, M., Lopes, F.B., McVey, C.E., Bustelo, X.R.X.R., Simas, J.P., de Miranda, M.P., Lopes, F.B., McVey, C.E., Bustelo, X.R.X.R., and Pedro Simas, J. (2013). Role of Src Homology Domain Binding in Signaling Complexes Assembled by the Murid gamma-Herpesvirus M2 Protein. J Biol Chem *288*, 3858-3870.

61. Sattler, M., Pride, Y.B., Quinnan, L.R., Verma, S., Malouf, N.A., Husson, H., Salgia, R., Lipkowitz, S., and Griffin, J.D. (2002). Differential expression and signaling of CBL and CBL-B in BCR/ABL transformed cells. Oncogene *21*, 1423-1433.

62. Miura-Shimura, Y., Duan, L., Rao, N.L., Reddi, A.L., Shimura, H., Rottapel, R., Druker, B.J., Tsygankov, A., Band, V., and Band, H. (2003). Cbl-mediated ubiquitinylation and negative regulation of Vav. J Biol Chem *278*, 38495-38504.

63. Duan, L., Raja, S.M., Chen, G., Virmani, S., Williams, S.H., Clubb, R.J., Mukhopadhyay, C., Rainey, M.A., Ying, G., Dimri, M.*, et al.* (2011). Negative regulation of EGFR-Vav2 signaling axis by Cbl ubiquitin ligase controls EGF receptor-mediated epithelial cell adherens junction dynamics and cell migration. Journal of Biological Chemistry.

64. Sebban, S., Farago, M., Gashai, D., Ilan, L., Pikarsky, E., Ben-Porath, I., and Katzav, S. (2013). Vav1 Fine Tunes p53 Control of Apoptosis versus Proliferation in Breast Cancer. PLoS ONE *8*.

65. Lawson, B.R., Manenkova, Y., Ahamed, J., Chen, X., Zou, J.-P., Baccala, R., Theofilopoulos, A.N., and Yuan, C. (2007). Inhibition of Transmethylation Down-Regulates CD4 T Cell Activation and Curtails Development of Autoimmunity in a Model System. J Immunol *178*, 5366-5374.

66. Choudhary, C., Kumar, C., Gnad, F., Nielsen, M.L., Rehman, M., Walther, T.C., Olsen, J.V., and Mann, M. (2009). Lysine acetylation targets protein complexes and co-regulates major cellular functions. Science *325*, 834-840.

67. Hansen, B.K., Gupta, R., Baldus, L., Lyon, D., Narita, T., Lammers, M., Choudhary, C., and Weinert, B.T. (2019). Analysis of human acetylation stoichiometry defines mechanistic constraints on protein regulation. Nat Commun *10*, 1055.

68. Mertins, P., Qiao, J.W., Patel, J., Udeshi, N.D., Clauser, K.R., Mani, D.R., Burgess, M.W., Gillette, M.A., Jaffe, J.D., and Carr, S.A. (2013). Integrated proteomic analysis of post-translational modifications by serial enrichment. Nat Methods *10*, 634-637.

69. Svinkina, T., Gu, H., Silva, J.C., Mertins, P., Qiao, J., Fereshetian, S., Jaffe, J.D., Kuhn, E., Udeshi, N.D., and Carr, S.A. (2015). Deep, Quantitative Coverage of the Lysine Acetylome Using Novel Anti-acetyl-lysine Antibodies and an Optimized Proteomic Workflow. Mol Cell Proteomics *14*, 2429-2440.

70. Weinert, B.T., Narita, T., Satpathy, S., Srinivasan, B., Hansen, B.K., Scholz, C., Hamilton, W.B., Zucconi, B.E., Wang, W.W., Liu, W.R., *et al.* (2018). Time-Resolved Analysis Reveals Rapid Dynamics and Broad Scope of the CBP/p300 Acetylome. Cell *174*, 231-244 e212.

71. Katzav, S., Martin-Zanca, D., and Barbacid, M. (1989). Vav, a Novel Human Oncogene Derived From a Locus Ubiquitously Expressed in Hematopoietic Cells. EMBO J *8*, 2283-2290.

72. Tarakhovsky, A., Turner, M., Schaal, S., Mee, P.J., Duddy, L.P., Rajewsky, K., and Tybulewicz, V.L.J. (1995). Defective antigen receptor-mediated proliferation of B and T cells in the absence of Vav. Nature *374*, 467-470.

73. Fischer, K.D., Zmuidzinas, A., Gardner, S., Barbacid, M., Bernstein, A., and Guidos, C. (1995). Defective T-cell receptor signalling and positive selection of Vav-deficient CD4+ CD8+ thymocytes. In Nature, pp. 474-477.

74. Turner, M., Mee, P.J., Walters, A.E., Quinn, M.E., Mellor, A.L., Zamoyska, R., and Tybulewicz, V.L.J. (1997). A requirement for the Rho-family GTP exchange factor Vav in positive and negative selection of thymocytes. Immunity *7*, 451-460.

75. Turner, M., and Billadeau, D.D. (2002). VAV proteins as signal integrators for multi-subunit immune-recognition receptors. Nat Rev Immunol *2*, 476-486.

76. Tybulewicz, V.L.J. (2005). Vav-family proteins in T-cell signalling. Curr Opin Immunol *17*, 267-274.

77. Fabbiano, S., Menacho-Marquez, M., Robles-Valero, J., Pericacho, M., Matesanz-Marin, A., Garcia-Macias, C., Sevilla, M.A., Montero, M.J., Alarcon, B., Lopez-Novoa, J.M., *et al.* (2015). Immunosuppression-Independent Role of Regulatory T Cells against Hypertension-Driven Renal Dysfunctions. Mol Cell Biol *35*, 3528-3546.

78. Kassem, S., Gaud, G., Bernard, I., Benamar, M., Dejean, A.S., Liblau, R., Fournie, G.J., Colacios, C., Malissen, B., and Saoudi, A. (2016). A Natural Variant of the T Cell Receptor-Signaling Molecule Vav1 Reduces Both Effector T Cell Functions and Susceptibility to Neuroinflammation. PLoS Genet *12*, e1006185.

79. Bernard, I., Sacquin, A., Kassem, S., Benamar, M., Colacios, C., Gador, M., Perals, C., Fazilleau, N., and Saoudi, A. (2018). A Natural Variant of the Signaling Molecule Vav1 Enhances Susceptibility to Myasthenia Gravis and Influences the T Cell Receptor Repertoire. Front Immunol *9*, 2399.

80. Colacios, C., Casemayou, A., Dejean, A.S., Gaits-Iacovoni, F., Pedros, C., Bernard, I., Lagrange, D., Deckert, M., Lamouroux, L., Jagodic, M., *et al.* (2011). The p.Arg63Trp polymorphism controls Vav1 functions and Foxp3 regulatory T cell development. J Exp Med *208*, 2183-2191.

81. Vigorito, E., Gambardella, L., Colucci, F., McAdam, S., and Turner, M. (2005). Vav proteins regulate peripheral B-cell survival. Blood *106*, 2391-2398.

82. Fujikawa, K., Miletic, A.V., Alt, F.W., Faccio, R., Brown, T., Hoog, J., Fredericks, J., Nishi, S., Mildiner, S., Moores, S.L., *et al.* (2003). Vav1/2/3-null Mice Define an Essential Role for Vav Family Proteins in Lymphocyte Development and Activation but a Differential Requirement in MAPK Signaling in T and B Cells. The Journal of Experimental Medicine.

83. Doody, G.M., Bell, S.E., Vigorito, E., Clayton, E., McAdam, S., Tooze, R., Fernandez, C., Lee, I.J., and Turner, M. (2001). Signal transduction through Vav-2 participates in humoral immune responses and B cell maturation. Nat Immunol.

84. Tedford, K., Nitschke, L., Girkontaite, I., Charlesworth, A., Chan, G., Sakk, V., Barbacid, M., and Fischer, K.D. (2001). Compensation between Vav-1 and Vav-2 in B cell development and antigen receptor signaling. Nat Immunol *2*, 548-555.

85. Faccio, R., Teitelbaum, S.L., Fujikawa, K., Chappel, J., Zallone, A., Tybulewicz, V.L., Ross, F.P., and Swat, W. (2005). Vav3 regulates osteoclast function and bone mass. Nature Medicine.

86. Yu, J., Yun, H., Shin, B., Kim, Y., Park, E.S., Choi, S., Yu, J., Amarasekara, D.S., Kim, S., Inoue, J., *et al.* (2016). Interaction of Tumor Necrosis Factor Receptor-associated Factor 6 (TRAF6) and Vav3 in the Receptor Activator of Nuclear Factor

kappaB (RANK) Signaling Complex Enhances Osteoclastogenesis. J Biol Chem *291*, 20643-20660.

87. Roth, S., Bergmann, H., Jaeger, M., Yeroslaviz, A., Neumann, K., Koenig, P.A., Prazeres da Costa, C., Vanes, L., Kumar, V., Johnson, M., *et al.* (2016). Vav Proteins Are Key Regulators of Card9 Signaling for Innate Antifungal Immunity. Cell Reports *17*, 2572-2583.

88. Cowan, C.W., Shao, Y.R., Sahin, M., Shamah, S.M., Lin, M.Z., Greer, P.L., Gao, S., Griffith, E.C., Brugge, J.S., and Greenberg, M.E. (2005). Vav family GEFs link activated Ephs to endocytosis and axon guidance. Neuron *46*, 205-217.

89. Shao, Y.R. (2007). Regulation of axon guidance and dendritic spine development by Vav family GEFs. In ProQuest Dissertations and Theses, pp. 105.

90. Moon, M.s., and Gomez, T.M. (2010). Balanced Vav2 GEF activity regulates neurite outgrowth and branching in vitro and in vivo. Mol Cell Neurosci *44*, 118-128.

91. Hale, C.F., Dietz, K.C., Varela, J.A., Wood, C.B., Zirlin, B.C., Leverich, L.S., Greene, R.W., and Cowan, C.W. (2011). Essential Role for Vav Guanine Nucleotide Exchange Factors in Brain-Derived Neurotrophic Factor-Induced Dendritic Spine Growth and Synapse Plasticity. J Neurosci *31*, 12426-12436.

92. Quevedo, C., Sauzeau, V., Menacho-Marquez, M., Castro-Castro, A., and Bustelo, X.R. (2010). Vav3-deficient Mice Exhibit a Transient Delay in Cerebellar Development. Mol Biol Cell *21*, 1125-1139.

93. Sauzeau, V., Horta-Junior, J.A.C., Riolobos, A.S., Fernández, G., Sevilla, M.A., Ló Pez, D.E., Montero, M.J., Rico, B., and Bustelo, X.R. (2010). Vav3 Is Involved in GABAergic Axon Guidance Events Important for the Proper Function of Brainstem Neurons Controlling Cardiovascular, Respiratory, and Renal Parameters. Mol Biol Cell *21*, 4251-4263.

94. Guyenet, P.G. (2006). The sympathetic control of blood pressure. Nature reviews *7*, 335-346.

95. Sauzeau, V., Sevilla, M.A., Rivas-Elena, J.V., De Álava, E., Montero, M.J., López-Novoa, J.M., and Bustelo, X.R. (2006). Vav3 proto-oncogene deficiency leads to sympathetic hyperactivity and cardiovascular dysfunction. Nat Med *12*, 841-845.

96. Menacho-Marquez, M., Nogueiras, R., Fabbiano, S., Sauzeau, V., Al-Massadi, O., Dieguez, C., and Bustelo, X.R. (2013). Chronic sympathoexcitation through loss of Vav3, a Rac1 activator, results in divergent effects on metabolic syndrome and obesity depending on diet. Cell Metab *18*, 199-211.

97. Lorenzo-Martin, L.F., Menacho-Marquez, M., Fabbiano, S., Al-Massadi, O., Abad, A., Rodriguez-Fdez, S., Sevilla, M.A., Montero, M.J., Dieguez, C., Nogueiras, R., *et al.* (2019). Vagal afferents contribute to sympathoexcitation-driven metabolic dysfunctions. J Endocrinol *240*, 483-496.

98. Ulc, A., Zeug, A., Bauch, J., van Leeuwen, S., Kuhlmann, T., Ffrench-Constant, C., Ponimaskin, E., and Faissner, A. (2019). The guanine nucleotide exchange factor Vav3 modulates oligodendrocyte precursor differentiation and supports remyelination in white matter lesions. Glia *67*, 376-392.

99. Zhu, S., Zhao, C., Wu, Y., Yang, Q., Shao, A., Wang, T., Wu, J., Yin, Y., Li, Y., Hou, J., *et al.* (2015). Identification of a Vav2-dependent mechanism for GDNF/Ret control of mesolimbic DAT trafficking. Nat Neurosci *18*, 1084-1093.

100. Sauzeau, V., Jerkic, M., Lopez-Novoa, J.M., and Bustelo, X.R. (2007). Loss of Vav2 proto-oncogene causes tachycardia and cardiovascular disease in mice. Mol Biol Cell *18*, 943-952.

101. Sauzeau, V., Sevilla, M.A., Montero, M.J., and Bustelo, X.R. (2010). The Rho/Rac exchange factor Vav2 controls nitric oxide-dependent responses in mouse vascular smooth muscle cells. J Clin Invest *120*, 315-330.

102. Fabbiano, S., Menacho-Marquez, M., Sevilla, M.A., Albarran-Juarez, J., Zheng, Y., Offermanns, S., Montero, M.J., and Bustelo, X.R. (2014). Genetic dissection of the vav2-rac1 signaling axis in vascular smooth muscle cells. Mol Cell Biol *34*, 4404-4419.

103. Jagodic, M., Colacios, C., Nohra, R., Dejean, A.S., Beyeen, A.D., Khademi, M., Casemayou, A., Lamouroux, L., Duthoit, C., Papapietro, O., *et al.* (2009). A role for VAV1 in experimental autoimmune encephalomyelitis and multiple sclerosis. Sci Transl Med *1*, 10ra21.

104. Fujikawa, K., Iwata, T., Inoue, K., Akahori, M., Kadotani, H., Fukaya, M., Watanabe, M., Chang, Q., Barnett, E.M., and Swat, W. (2010). VAV2 and VAV3 as candidate disease genes for spontaneous glaucoma in mice and humans. PLoS ONE *5*.

105. Shi, X., Huang, T., Wang, J., Liang, Y., Gu, C., Xu, Y., Sun, J., Lu, Y., Sun, K., Chen, S., *et al.* (2018). Next-generation sequencing identifies novel genes with rare variants in total anomalous pulmonary venous connection. EBioMedicine *38*.

106. Aleksic, B., Kushima, I., Hashimoto, R., Ohi, K., Ikeda, M., Yoshimi, A., Nakamura, Y., Ito, Y., Okochi, T., Fukuo, Y., *et al.* (2013). Analysis of the VAV3 as candidate gene for schizophrenia: Evidences from voxel-based morphometry and mutation screening. Schizophrenia Bulletin *39*, 720-728.

107. Eriksson, N., Tung, J.Y., Kiefer, A.K., Hinds, D.A., Francke, U., Mountain, J.L., and Do, C.B. (2012). Novel associations for hypothyroidism include known autoimmune risk loci. PLoS ONE.

108. Kwak, S.H., Park, Y.J., Go, M.J., Lee, K.E., Kim, S.J., Choi, H.S., Kim, T.H., HeeChoi, S., Lim, S., Kim, K.W.*, et al.* (2014). A genome-wide association study on thyroid function and anti-thyroid peroxidase antibodies in Koreans. Hum Mol Genet *23*, 4433-4442.

109. Oryoji, D., Ueda, S., Yamamoto, K., Noh, J.Y., Okamura, K., Noda, M., Watanabe, N., Yoshihara, A., Ito, K., and Sasazuki, T. (2015). Identification of a hashimoto thyroiditis susceptibility locus via a genome-wide comparison with graves' disease. J Clin Endocrinol Metab *100*, 319-324.

110. Hornstein, I., Pikarsky, E., Groysman, M., Amir, G., Peylan-Ramu, N., and Katzav, S. (2003). The haematopoietic specific signal transducer Vav1 is expressed in a subset of human neuroblastomas. J Pathol *199*, 526-533.

111. Lindsey, J.C., Kawauchi, D., Schwalbe, E.C., Solecki, D.J., Selby, M.P., McKinnon, P.J., Olson, J.M., Hayden, J.T., Grundy, R.G., Ellison, D.W.*, et al.* (2015). Cross-species epigenetics identifies a critical role for VAV1 in SHH subgroup medulloblastoma maintenance. Oncogene *34*, 4746-4757.

112. Fernandez-Zapico, M.E., Gonzalez-Paz, N.C., Weiss, E., Savoy, D.N., Molina, J.R., Fonseca, R., Smyrk, T.C., Chari, S.T., Urrutia, R., and Billadeau, D.D. (2005). Ectopic expression of VAV1 reveals an unexpected role in pancreatic cancer tumorigenesis. Cancer Cell.

113. Grassilli, S., Brugnoli, F., Lattanzio, R., Rossi, C., Perracchio, L., Mottolese, M., Marchisio, M., Palomba, M., Nika, E., Natali, P.G.*, et al.* (2014). High nuclear level of Vav1 is a positive prognostic factor in early invasive breast tumors: a role in modulating genes related to the efficiency of metastatic process. Oncotarget *5*, 4320-4336.

114. Lazer, G., Pe'er, L., Farago, M., Machida, K., Mayer, B.J., and Katzav, S. (2010). Tyrosine residues at the carboxyl terminus of Vav1 play an important role in regulation of its biological activity. J Biol Chem *285*, 23075-23085.

115. Campbell, J.D., Alexandrov, A., Kim, J., Wala, J., Berger, A.H., Pedamallu, C.S., Shukla, S.A., Guo, G., Brooks, A.N., Murray, B.A.*, et al.* (2016). Distinct patterns of somatic genome alterations in lung adenocarcinomas and squamous cell carcinomas. Nat Genet *48*, 607-616.

116. Citterio, C., Menacho-Márquez, M., García-Escudero, R., Larive, R.M., Barreiro, O., Sánchez-Madrid, F., Paramio, J.M., and Bustelo, X.R. (2012). The rho

exchange factors vav2 and vav3 control a lung metastasis-specific transcriptional program in breast cancer cells. Science Signaling *5*.

117. Lorenzo-Martín, L.F., Citterio, C., Menacho-Márquez, M., Conde, J., Larive, R.M., Rodríguez-Fdez, S., García-Escudero, R., Robles-Valero, J., Cuadrado, M., Fernández-Pisonero, I.*, et al.* (2018). Vav proteins maintain epithelial traits in breast cancer cells using miR-200c-dependent and independent mechanisms. Oncogene *38*, 209-227.

118. Menacho-Márquez, M., García-Escudero, R., Ojeda, V., Abad, A., Delgado, P., Costa, C., Ruiz, S., Alarcón, B., Paramio, J.M., and Bustelo, X.R. (2013). The Rho Exchange Factors Vav2 and Vav3 Favor Skin Tumor Initiation and Promotion by Engaging Extracellular Signaling Loops. PLoS Biology *11*.

119. Dong, Z., Liu, Y., Lu, S., Wang, A., Lee, K., Wang, L.-H., and Revelo, M. (2006). Vav3 oncogene is overexpressed and regulates cell growth and androgen receptor activity in human prostate cancer. Mol Endocrinol *20*, 2315-2325.

120. Lyons, L.S., and Burnstein, K.L. (2006). Vav3, a Rho GTPase guanine nucleotide exchange factor, increases during progression to androgen independence in prostate cancer cells and potentiates androgen receptor transcriptional activity. Mol Endocrinol *20*, 1061-1072.

121. Abate, F., da Silva-Almeida, A.C., Zairis, S., Robles-Valero, J., Couronne, L., Khiabanian, H., Quinn, S.A., Kim, M.-Y., Laginestra, M.A., Kim, C.*, et al.* (2017). Activating mutations and translocations in the guanine exchange factor VAV1 in peripheral T-cell lymphomas. Proc Natl Acad Sci U S A *114*, 764-769.

122. Boddicker, R.L., Razidlo, G.L., Dasari, S., Zeng, Y., Hu, G., Knudson, R.A., Greipp, P.T., Davila, J.I., Johnson, S.H., Porcher, J.C.*, et al.* (2016). Integrated mate-pair and RNA sequencing identifies novel, targetable gene fusions in peripheral T-cell lymphoma. Blood *128*, 1234-1245.

123. Kataoka, K., Nagata, Y., Kitanaka, A., Shiraishi, Y., Shimamura, T., Yasunaga, J.I., Totoki, Y., Chiba, K., Sato-Otsubo, A., Nagae, G.*, et al.* (2015). Integrated molecular analysis of adult T cell leukemia/lymphoma. Nat Genet *47*, 1304-1315.

124. Vallois, D., Dobay, M.P.D., Morin, R.D., Lemonnier, F., Missiaglia, E., Juilland, M., Iwaszkiewicz, J., Fataccioli, V., Bisig, B., Roberti, A.*, et al.* (2016). Activating mutations in genes related to TCR signaling in angioimmunoblastic and other follicular helper T-cell-derived lymphomas. Blood *128*, 1490-1502.

125. Bassermann, F., Jahn, T., Miething, C., Seipel, P., Bai, R.Y., Coutinho, S., Tybulewicz, V.L., Peschel, C., and Duyster, J. (2002). Association of Bcr-Abl with the proto-oncogene Vav is implicated in activation of the Rac-1 pathway. J Biol Chem *277*, 12437-12445.

126. Chang, K.H., Sanchez-Aguilera, A., Shen, S., Sengupta, A., Madhu, M.N., Ficker, A.M., Dunn, S.K., Kuenzi, A.M., Arnett, J.L., Santho, R.A., *et al.* (2012). Vav3 collaborates with p190-BCR-ABL in lymphoid progenitor leukemogenesis, proliferation, and survival. Blood *120*, 800-811.

127. Martin, H., Mali, R.S., Ma, P., Chatterjee, A., Ramdas, B., Sims, E., Munugalavadla, V., Ghosh, J., Mattingly, R.R., Visconte, V., *et al.* (2013). Pak and Rac GTPases promote oncogenic KIT-induced neoplasms. J Clin Invest *123*, 4449-4463.

128. Spiegelman, B.M., and Flier, J.S. (2001). Obesity and the regulation of energy balance. Cell *104*, 531-543.

129. Lempradl, A., Pospisilik, J.A., and Penninger, J.M. (2015). Exploring the emerging complexity in transcriptional regulation of energy homeostasis. Nat Rev Genet *16*, 665-681.

130. Steinert, R.E., Feinle-Bisset, C., Asarian, L., Horowitz, M., Beglinger, C., and Geary, N. (2017). Ghrelin, CCK, GLP-1, and PYY(3-36): Secretory Controls and Physiological Roles in Eating and Glycemia in Health, Obesity, and After RYGB. Physiol Rev *97*, 411-463.

131. Czech, M.P. (2017). Insulin action and resistance in obesity and type 2 diabetes. Nat Med *23*, 804-814.

132. Christoffolete, M.A., Silva, W.J., Ramos, G.V., Bento, M.R., Costa, M.O., Ribeiro, M.O., Okamoto, M.M., Lohmann, T.H., Machado, U.F., Musaro, A., *et al.* (2015). Muscle IGF-1-induced skeletal muscle hypertrophy evokes higher insulin sensitivity and carbohydrate use as preferential energy substrate. Biomed Res Int *2015*, 282984.

133. Chung, H.S., and Choi, K.M. (2018). Adipokines and Myokines: A Pivotal Role in Metabolic and Cardiovascular Disorders. Curr Med Chem *25*, 2401-2415.

134. Oh, K.J., Lee, D.S., Kim, W.K., Han, B.S., Lee, S.C., and Bae, K.H. (2016). Metabolic Adaptation in Obesity and Type II Diabetes: Myokines, Adipokines and Hepatokines. Int J Mol Sci *18*.

135. Seematter, G., Binnert, C., Martin, J.L., and Tappy, L. (2004). Relationship between stress, inflammation and metabolism. Curr Opin Clin Nutr Metab Care *7*, 169-173.

136. Schiaffino, S., and Mammucari, C. (2011). Regulation of skeletal muscle growth by the IGF1-Akt/PKB pathway: insights from genetic models. Skelet Muscle *1*, 4.

137. Taniguchi, C.M., Emanuelli, B., and Kahn, C.R. (2006). Critical nodes in signalling pathways: insights into insulin action. Nat Rev Mol Cell Biol *7*, 85-96.

138. Wu, H., and Ballantyne, C.M. (2017). Skeletal muscle inflammation and insulin resistance in obesity. J Clin Invest *127*, 43-54.

139. Petersen, K.F., and Shulman, G.I. (2002). Pathogenesis of skeletal muscle insulin resistance in type 2 diabetes mellitus. Am J Cardiol *90*, 11G-18G.

140. Pedersen, B.K., and Febbraio, M.A. (2012). Muscles, exercise and obesity: skeletal muscle as a secretory organ. Nat Rev Endocrinol *8*, 457-465.

141. Pedersen, B.K. (2019). Physical activity and muscle-brain crosstalk. Nat Rev Endocrinol.

142. Camporez, J.P., Petersen, M.C., Abudukadier, A., Moreira, G.V., Jurczak, M.J., Friedman, G., Haqq, C.M., Petersen, K.F., and Shulman, G.I. (2016). Anti-myostatin antibody increases muscle mass and strength and improves insulin sensitivity in old mice. Proc Natl Acad Sci U S A *113*, 2212-2217.

143. DeFronzo, R.A., and Tripathy, D. (2009). Skeletal muscle insulin resistance is the primary defect in type 2 diabetes. Diabetes care *32*, 157-163

144. Son, J.W., Lee, S.S., Kim, S.R., Yoo, S.J., Cha, B.Y., Son, H.Y., and Cho, N.H. (2017). Low muscle mass and risk of type 2 diabetes in middle-aged and older adults: findings from the KoGES. Diabetologia *60*, 865-872.

145. Kowluru, A. (2017). Role of G-proteins in islet function in health and diabetes. Diabetes Obes Metab *19*, 63-75.

146. Ueda, S., Kitazawa, S., Ishida, K., Nishikawa, Y., Matsui, M., Matsumoto, H., Aoki, T., Nozaki, S., Takeda, T., Tamori, Y.*, et al.* (2010). Crucial role of the small GTPase Rac1 in insulin-stimulated translocation of glucose transporter 4 to the mouse skeletal muscle sarcolemma. FASEB J *24*, 2254-2261.

147. Sylow, L., Kleinert, M., Pehmoller, C., Prats, C., Chiu, T.T., Klip, A., Richter, E.A., and Jensen, T.E. (2014). Akt and Rac1 signaling are jointly required for insulin-stimulated glucose uptake in skeletal muscle and downregulated in insulin resistance. Cell Signal *26*, 323-331.

148. Sylow, L., Møller, L.L.V., Kleinert, M., Richter, E.A., and Jensen, T.E. (2014). Rac1 - a novel regulator of contraction-stimulated glucose uptake in skeletal muscle. Exp Physiol *99*, 1574-1580.

149. Sylow, L., Møller, L.L.V., D'Hulst, G., Schjerling, P., Jensen, T.E., and Richter, E.A. (2016). Rac1 in muscle is dispensable for improved insulin action after exercise in mice. Endocrinology *157*, 3009-3015.

150. Sylow, L., Møller, L.L.V., Kleinert, M., D'Hulst, G., De Groote, E., Schjerling, P., Steinberg, G.R., Jensen, T.E., and Richter, E.A. (2017). Rac1 and AMPK account for the majority of muscle glucose uptake stimulated by ex vivo contraction but not in vivo exercise. Diabetes *66*, 1548-1559.

151. Ueda, S., Kataoka, T., and Satoh, T. (2008). Activation of the small GTPase Rac1 by a specific guanine-nucleotide-exchange factor suffices to induce glucose uptake into skeletal-muscle cells. Biol Cell *100*, 645-657.

152. Chiu, T.T., Jensen, T.E., Sylow, L., Richter, E.A., and Klip, A. (2011). Rac1 signalling towards GLUT4/glucose uptake in skeletal muscle. Cell Signal *23*, 1546-1554.

153. Nozaki, S., Takeda, T., Kitaura, T., Takenaka, N., Kataoka, T., and Satoh, T. (2013). Akt2 regulates Rac1 activity in the insulin-dependent signaling pathway leading to GLUT4 translocation to the plasma membrane in skeletal muscle cells. Cell Signal *25*, 1361-1371.

154. Takenaka, N., Yasuda, N., Nihata, Y., Hosooka, T., Noguchi, T., Aiba, A., and Satoh, T. (2014). Role of the guanine nucleotide exchange factor in Akt2-mediated plasma membrane translocation of GLUT4 in insulin-stimulated skeletal muscle. Cell Signal *26*, 2460-2469.

155. Satoh, T. (2014). Rho GTPases in insulin-stimulated glucose uptake. Small GTPases *5*, 28102.

156. Lee, D.H., Shi, J., Jeoung, N.H., Kim, M.S., Zabolotny, J.M., Lee, S.W., White, M.F., Wei, L., and Kim, Y.-B. (2009). Targeted disruption of ROCK1 causes insulin resistance in vivo. J Biol Chem *284*, 11776-11780.

157. Chun, K.-H., Choi, K.-D., Lee, D.-H., Jung, Y., Henry, R.R., Ciaraldi, T.P., and Kim, Y.-B. (2011). In vivo activation of ROCK1 by insulin is impaired in skeletal muscle of humans with type 2 diabetes. Am J Physiol Endocrinol Metab *300*, 536-542.

158. Furukawa, N., Ongusaha, P., Jahng, W.J., Araki, K., Choi, C.S., Kim, H.J., Lee, Y.H., Kaibuchi, K., Kahn, B.B., Masuzaki, H.*, et al.* (2005). Role of Rho-kinase in regulation of insulin action and glucose homeostasis. Cell Metabolism.

159. Lee, S.-H., Huang, H., Choi, K., Lee, D.H., Shi, J., Liu, T., Chun, K.H., Seo, J.A., Lima, I.S., Zabolotny, J.M.*, et al.* (2014). ROCK1 isoform-specific deletion reveals a role for diet-induced insulin resistance. Am J Physiol Endocrinol Metab *306*, 332-343.

160. Zhou, X., Li, R., Liu, X., Wang, L., Hui, P., Chan, L., Saha, P.K., and Hu, Z. (2016). ROCK1 reduces mitochondrial content and irisin production in muscle suppressing adipocyte browning and impairing insulin sensitivity. Sci Rep *6*, 29669.

161. Schiaffino, S., Dyar, K.A., Ciciliot, S., Blaauw, B., and Sandri, M. (2013). Mechanisms regulating skeletal muscle growth and atrophy. FEBS J *280*, 4294-4314.

162. Garcia-Prat, L., Sousa-Victor, P., and Munoz-Canoves, P. (2017). Proteostatic and Metabolic Control of Stemness. Cell Stem Cell *20*, 593-608.

163. Yin, H., Price, F., and Rudnicki, M.A. (2013). Satellite Cells and the Muscle Stem Cell Niche. Physiol Rev *93*, 23-67.

164. Egerman, M.A., and Glass, D.J. (2014). Signaling pathways controlling skeletal muscle mass. Crit Rev Biochem Mol Biol *49*, 59-68.

165. Accili, D., Drago, J., Lee, E.J., Johnson, M.D., Cool, M.H., Salvatore, P., Asico, L.D., Jose, P.A., Taylor, S.I., and Westphal, H. (1996). Early neonatal death in mice homozygous for a null allele of the insulin receptor gene. Nat Genet *12*, 106-109.

166. Joshi, R.L., Lamothe, B., Cordonnier, N., Mesbah, K., Monthioux, E., Jami, J., and Bucchini, D. (1996). Targeted disruption of the insulin receptor gene in the mouse results in neonatal lethality. EMBO J *15*, 1542-1547.

167. Belfiore, A., Frasca, F., Pandini, G., Sciacca, L., and Vigneri, R. (2009). Insulin receptor isoforms and insulin receptor/insulin-like growth factor receptor hybrids in physiology and disease. Endocr Rev *30*, 586-623.

168. Trendelenburg, A.U., Meyer, A., Rohner, D., Boyle, J., Hatakeyama, S., and Glass, D.J. (2009). Myostatin reduces Akt/TORC1/p70S6K signaling, inhibiting myoblast differentiation and myotube size. Am J Physiol Cell Physiol *296*, 1258-1270.

169. Rommel, C., Bodine, S.C., Clarke, B.A., Rossman, R., Nunez, L., Stitt, T.N., Yancopoulos, G.D., and Glass, D.J. (2001). Mediation of IGF-1-induced skeletal myotube hypertrophy by Pl(3)K/Alt/mTOR and Pl(3)K/Akt/GSK3 pathways. Nat Cell Biol *3*, 1009-1013.

170. O'Neill, B.T., Lauritzen, H.P., Hirshman, M.F., Smyth, G., Goodyear, L.J., and Kahn, C.R. (2015). Differential Role of Insulin/IGF-1 Receptor Signaling in Muscle Growth and Glucose Homeostasis. Cell Rep *11*, 1220-1235.

171. Hamrick, M.W., Pennington, C., Webb, C.N., and Isales, C.M. (2006). Resistance to body fat gain in 'double-muscled' mice fed a high-fat diet. Int J Obes *30*, 868-870.

172. Guo, T., Jou, W., Chanturiya, T., Portas, J., Gavrilova, O., and McPherron, A.C. (2009). Myostatin inhibition in muscle, but not adipose tissue, decreases fat mass and improves insulin sensitivity. PLoS ONE.

173. Le Grand, F., and Rudnicki, M.A. (2007). Skeletal muscle satellite cells and adult myogenesis. Curr Opin Cell Biol *19*, 628-633.

174. Zammit, P.S. (2017). Function of the myogenic regulatory factors Myf5, MyoD, Myogenin and MRF4 in skeletal muscle, satellite cells and regenerative myogenesis. Semin Cell Dev Biol *72*, 19-32.

175. Castellani, L., Salvati, E., Alemà, S., and Falcone, G. (2006). Fine regulation of RhoA and Rock is required for skeletal muscle differentiation. J Biol Chem *281*, 15249-15257.

176. Charrasse, S., Comunale, F., Grumbach, Y., Poulat, F., Blangy, A., and Gauthier-Rouvière, C. (2006). RhoA GTPase Regulates M-Cadherin Activity and Myoblast Fusion. Mol Biol Cell *17*, 749-759.

177. Charrasse, S., Meriane, M., Comunale, F., Blangy, A., and Gauthier-Rouvière, C. (2002). N-cadherin-dependent cell-cell contact regulates Rho GTPases and β-catenin localization in mouse C2C12 myoblasts. J Cell Biol *158*, 953-965.

178. Doherty, J.T., Lenhart, K.C., Cameron, M.V., Mack, C.P., Conlon, F.L., and Taylor, J.M. (2011). Skeletal muscle differentiation and fusion are regulated by the BAR-containing Rho-GTPase-activating Protein (Rho-GAP), GRAF. Journal of Biological Chemistry *286*, 25903-25921.

179. Fortier, M., Comunale, F., Kucharczak, J., Blangy, A., Charrasse, S., and Gauthier-Rouvière, C. (2008). RhoE controls myoblast alignment prior fusion through RhoA and ROCK. Cell Death and Differentiation *15*, 1221-1231.

180. Charrasse, S., Comunale, F., Fortier, M., Portales-Casamar, E., Debant, A., and Gauthier-Rouvière, C. (2007). M-Cadherin Activates Rac1 GTPase through the Rho-GEF Trio during Myoblast Fusion. Mol Biol Cell *18*, 1734-1743.

181. Haralalka, S., Shelton, C., Cartwright, H.N., Katzfey, E., Janzen, E., and Abmayr, S.M. (2013). Asymmetric Mbc, active Rac1 and F-actin foci in the fusion-competent myoblasts during myoblast fusion in Drosophila. Development *138*, 1551-1562.

182. Joseph, G.A., Lu, M., Radu, M., Lee, J.K., Burden, S.J., Chernoff, J., and Krauss, R.S. (2017). Group I Paks Promote Skeletal Myoblast Differentiation In Vivo and In Vitro. Mol Cell Biol *37*, 222-216.

183. Duan, R., Jin, P., Luo, F., Zhang, G., Anderson, N., and Chen, E.H. (2012). Group I PAKs function downstream of Rac to promote podosome invasion during myoblast fusion in vivo. Journal of Cell Biology.

184. Vasyutina, E., Martarelli, B., Brakebusch, C., Wende, H., and Birchmeier, C. (2009). The small G-proteins Rac1 and Cdc42 are essential for myoblast fusion in the mouse. Proc Natl Acad Sci U S A *106*, 8935-8940.

185. Laurin, M., Fradet, N., Blangy, A., Hall, A., Vuori, K., and Cote, J.-F. (2008). The atypical Rac activator Dock180 (Dock1) regulates myoblast fusion in vivo. Proc Natl Acad Sci U S A *105*, 15446-15451.

186. Moore, C.A., Parkin, C.A., Bidet, Y., and Ingham, P.W. (2007). A role for the Myoblast city homologues Dock1 and Dock5 and the adaptor proteins Crk and Crk-like in zebrafish myoblast fusion. Development *134*, 3145-3153.

187. Hamoud, N., Tran, V., Aimi, T., Kakegawa, W., Lahaie, S., Thibault, M.P., Pelletier, A., Wong, G.W., Kim, I.S., Kania, A.*, et al.* (2018). Spatiotemporal regulation of the GPCR activity of BAI3 by C1qL4 and Stabilin-2 controls myoblast fusion. Nat Commun *9*, 4470.

188. Hamoud, N., Tran, V., Croteau, L.P., Kania, A., and Cote, J.F. (2014). G-protein coupled receptor BAI3 promotes myoblast fusion in vertebrates. Proc Natl Acad Sci U S A *111*, 3745-3750.

189. O'Brien, S.P., Seipel, K., Medley, Q.G., Bronson, R., Segal, R., and Streuli, M. (2000). Skeletal muscle deformity and neuronal disorder in Trio exchange factor-deficient mouse embryos. Proc Natl Acad Sci U S A *97*, 12074-12078.

190. Ruiz, S., Santos, E., and Bustelo, X.R. (2007). RasGRF2, a guanosine nucleotide exchange factor for Ras GTPases, participates in T-cell signaling responses. Mol Cell Biol *27*, 8127-8142.

191. Edgar, R.C. (2004). MUSCLE: a multiple sequence alignment method with reduced time and space complexity. BMC Bioinformatics *5*, 113.

192. Edgar, R.C. (2004). MUSCLE: multiple sequence alignment with high accuracy and high throughput. Nucleic Acids Res *32*, 1792-1797.

193. Waterhouse, A.M., Procter, J.B., Martin, D.M., Clamp, M., and Barton, G.J. (2009). Jalview Version 2--a multiple sequence alignment editor and analysis workbench. Bioinformatics *25*, 1189-1191.

194. Guindon, S., Dufayard, J.F., Lefort, V., Anisimova, M., Hordijk, W., and Gascuel, O. (2010). New algorithms and methods to estimate maximum-likelihood phylogenies: assessing the performance of PhyML 3.0. Syst Biol *59*, 307-321.

195. Robles-Valero, J., Martín-Cófreces, N.B., Lamana, A., Macdonald, S., Volkov, Y., and Sánchez-Madrid, F. (2010). Integrin and CD3/TCR activation are regulated by the scaffold protein AKAP450. Blood *115*, 4174-4184.

196. Schultz, J., Milpetz, F., Bork, P., and Ponting, C.P. (1998). SMART, a simple modular architecture research tool: Identification of signaling domains. Proc Natl Acad Sci U S A *95*, 5857-5864.

197. Mortlock, D., Keller, E.B., Ziegra, C.J., and Suter, M.M. (1993). High efficiency transfection of monkey kidney COS-1 cells. J Tissue Cult Methods *15*, 176-180.

198. Shevchenko, A., Tomas, H., Havliš, J., Olsen, J.V., and Mann, M. (2007). In-gel digestion for mass spectrometric characterization of proteins and proteomes. Nat Protoc *1*, 2856-2860.

199. Rappsilber, J., Mann, M., and Ishihama, Y. (2007). Protocol for micro-purification, enrichment, pre-fractionation and storage of peptides for proteomics using StageTips. Nat Protoc *2*, 1896-1906.

200. Olsen, J.V., de Godoy, L.M.F., Li, G., Macek, B., Mortensen, P., Pesch, R., Makarov, A., Lange, O., Horning, S., and Mann, M. (2005). Parts per Million Mass Accuracy on an Orbitrap Mass Spectrometer via Lock Mass Injection into a C-trap. Mol Cell Proteomics *4*, 2010-2021.

201. MacLean, B., Tomazela, D.M., Shulman, N., Chambers, M., Finney, G.L., Frewen, B., Kern, R., Tabb, D.L., Liebler, D.C., and MacCoss, M.J. (2010). Skyline: an open source document editor for creating and analyzing targeted proteomics experiments. Bioinformatics *26*, 966-968.

202. Kim, J.Y., Kim, K.W., Kwon, H.J., Lee, D.W., and Yoo, J.S. (2002). Probing lysine acetylation with a modification-specific marker ion using high-performance liquid chromatography/electrospray-mass spectrometry with collision-induced dissociation. Anal Chem *74*, 5443-5449.

203. Ojeda, V., Castro-Castro, A., and Bustelo, X.R. (2014). Coronin1 proteins dictate rac1 intracellular dynamics and cytoskeletal output. Mol Cell Biol *34*, 3388-3406.

204. Rodrigues, L., Pires de Miranda, M., Caloca, M.J., Bustelo, X.R., and Simas, J.P. (2006). Activation of Vav by the gammaherpesvirus M2 protein contributes to the establishment of viral latency in B lymphocytes. J Virol *80*, 6123-6135.

205. Martinez-Sanchez, N., Seoane-Collazo, P., Contreras, C., Varela, L., Villarroya, J., Rial-Pensado, E., Buque, X., Aurrekoetxea, I., Delgado, T.C., Vazquez-Martinez, R.*, et al.* (2017). Hypothalamic AMPK-ER Stress-JNK1 Axis Mediates the Central Actions of Thyroid Hormones on Energy Balance. Cell Metab *26*, 212-229 e212.

206. Baecker, V. (2012). ImageJ macro tool sets for biological image analysis. Presented at the ImageJ User and Developer Conference.

207. Flajnik, M.F., and Kasahara, M. (2010). Origin and evolution of the adaptive immune system: genetic events and selective pressures. Nat Rev Genet *11*, 47-59.

208. Kuhne, M.R., Ku, G., and Weiss, A. (2000). A guanine nucleotide exchange factor-independent function of Vav1 in transcriptional activation. J Biol Chem *275*, 2185-2190.

209. Li, S.Y., Du, M.J., Wan, Y.J., Lan, B., Liu, Y.H., Yang, Y., Zhang, C.Z., and Cao, Y. (2013). The N-terminal 20-amino acid region of guanine nucleotide exchange factor Vav1 plays a distinguished role in T cell receptor-mediated calcium signaling. J Biol Chem *288*, 3777-3785.

210. Maxwell, K.N., Zhou, Y., and Hancock, J.F. (2018). Rac1 nanoscale organization on the plasma membrane is driven by lipid binding specificity encoded in the membrane anchor. Mol Cell Biol.

211. Zhou, Y., Prakash, P., Liang, H., Cho, K.J., Gorfe, A.A., and Hancock, J.F. (2017). Lipid-sorting specificity encoded in K-Ras membrane anchor regulates signal output. Cell *168*, 239-251 e216.

212. Ahearn, I.M., Haigis, K., Bar-Sagi, D., and Philips, M.R. (2011). Regulating the regulator: post-translational modification of RAS. Nat Rev Mol Cell Biol *13*, 39-51.

213. Lemmon, M.A. (2008). Membrane recognition by phospholipid-binding domains. Nat Rev Mol Cell Biol *9*, 99-111.

214. Niebuhr, K., Giuriato, S., Pedron, T., Philpott, D.J., Gaits, F., Sable, J., Sheetz, M.P., Parsot, C., Sansonetti, P.J., and Payrastre, B. (2002). Conversion of PtdIns(4,5)P(2) into PtdIns(5)P by the S.flexneri effector IpgD reorganizes host cell morphology. EMBO J *21*, 5069-5078.

215. Borchers, C., Parker, C.E., Deterding, L.J., and Tomer, K.B. (1999). Preliminary comparison of precursor scans and liquid chromatography-tandem mass spectrometry on a hybrid quadrupole time-of-flight mass spectrometer. In Journal of Chromatography A.

216. Song, E.H., Oh, W., Ulu, A., Carr, H.S., Zuo, Y., and Frost, J.A. (2015). Acetylation of the RhoA GEF Net1A controls its subcellular localization and activity. J Cell Sci *128*, 913-922.

217. Kim, S.C., Sprung, R., Chen, Y., Xu, Y., Ball, H., Pei, J., Cheng, T., Kho, Y., Xiao, H., Xiao, L.*, et al.* (2006). Substrate and functional diversity of lysine acetylation revealed by a proteomics survey. Mol Cell *23*, 607-618.

218. Chen, C.H., Martin, V.A., Gorenstein, N.M., Geahlen, R.L., and Post, C.B. (2011). Two closely spaced tyrosines regulate NFAT signaling in B cells via Syk association with Vav. Mol Cell Biol *31*, 2984-2996.

219. Chen, C.H., Piraner, D., Gorenstein, N.M., Geahlen, R.L., and Beth Post, C. (2013). Differential recognition of syk-binding sites by each of the two phosphotyrosine-binding pockets of the Vav SH2 domain. Biopolymers *99*, 897-907.

220. O'Neill, B.T., Lee, K.Y., Klaus, K., Softic, S., Krumpoch, M.T., Fentz, J., Stanford, K.I., Robinson, M.M., Cai, W., Kleinridders, A.*, et al.* (2016). Insulin and IGF-1 receptors regulate FoxO-mediated signaling in muscle proteostasis. J Clin Invest *126*, 3433-3446.

221. Bolsoni-Lopes, A., and Alonso-Vale, M.I. (2015). Lipolysis and lipases in white adipose tissue - An update. Arch Endocrinol Metab *59*, 335-342.

222. Chouchani, E.T., Kazak, L., and Spiegelman, B.M. (2019). New Advances in Adaptive Thermogenesis: UCP1 and Beyond. Cell Metab *29*, 27-37.

223. Hammond, G.R., Fischer, M.J., Anderson, K.E., Holdich, J., Koteci, A., Balla, T., and Irvine, R.F. (2012). PI4P and PI(4,5)P2 are essential but independent lipid determinants of membrane identity. Science *337*, 727-730.

224. Gozani, O., Karuman, P., Jones, D.R., Ivanov, D., Cha, J., Lugovskoy, A.A., Baird, C.L., Zhu, H., Field, S.J., Lessnick, S.L.*, et al.* (2003). The PHD finger of the chromatin-associated protein ING2 functions as a nuclear phosphoinositide receptor. Cell *114*, 99-111.

225. Stijf-Bultsma, Y., Sommer, L., Tauber, M., Baalbaki, M., Giardoglou, P., Jones, D.R., Gelato, K.A., van Pelt, J., Shah, Z., Rahnamoun, H.*, et al.* (2015). The basal transcription complex component TAF3 transduces changes in nuclear phosphoinositides into transcriptional output. Mol Cell *58*, 453-467.

226. Viiri, K.M., Janis, J., Siggers, T., Heinonen, T.Y., Valjakka, J., Bulyk, M.L., Maki, M., and Lohi, O. (2009). DNA-binding and -bending activities of SAP30L and SAP30 are mediated by a zinc-dependent module and monophosphoinositides. Mol Cell Biol *29*, 342-356.

227. Kaadige, M.R., and Ayer, D.E. (2006). The polybasic region that follows the plant homeodomain zinc finger 1 of Pf1 is necessary and sufficient for specific phosphoinositide binding. J Biol Chem *281*, 28831-28836.

228. Nunes, J.A., and Guittard, G. (2013). An Emerging Role for PI5P in T Cell Biology. Front Immunol *4*, 80.

229. Viaud, J., Mansour, R., Antkowiak, A., Mujalli, A., Valet, C., Chicanne, G., Xuereb, J.M., Terrisse, A.D., Severin, S., Gratacap, M.P., *et al.* (2016). Phosphoinositides: Important lipids in the coordination of cell dynamics. Biochimie *125*, 250-258.

230. Guittard, G., Gerard, A., Dupuis-Coronas, S., Tronchere, H., Mortier, E., Favre, C., Olive, D., Zimmermann, P., Payrastre, B., and Nunes, J.A. (2009). Cutting edge: Dok-1 and Dok-2 adaptor molecules are regulated by phosphatidylinositol 5-phosphate production in T cells. J Immunol *182*, 3974-3978.

231. Guittard, G., Mortier, E., Tronchere, H., Firaguay, G., Gerard, A., Zimmermann, P., Payrastre, B., and Nunes, J.A. (2010). Evidence for a positive role of PtdIns5P in T-cell signal transduction pathways. FEBS Lett *584*, 2455-2460.

232. DeFord-Watts, L.M., Dougall, D.S., Belkaya, S., Johnson, B.A., Eitson, J.L., Roybal, K.T., Barylko, B., Albanesi, J.P., Wulfing, C., and van Oers, N.S. (2011). The CD3 zeta subunit contains a phosphoinositide-binding motif that is required for the stable accumulation of TCR-CD3 complex at the immunological synapse. J Immunol *186*, 6839-6847.

233. Viaud, J., Lagarrigue, F., Ramel, D., Allart, S., Chicanne, G., Ceccato, L., Courilleau, D., Xuereb, J.M., Pertz, O., Payrastre, B., *et al.* (2014). Phosphatidylinositol 5-phosphate regulates invasion through binding and activation of Tiam1. Nat Commun *5*, 4080.

234. Caloca, M.J., Zugaza, J.L., Matallanas, D., Crespo, P., and Bustelo, X.R. (2003). Vav mediates Ras stimulation by direct activation of the GDP/GTP exchange factor Ras GRP1. EMBO J *22*, 3326-3336.

235. Reynolds, L.F., de Bettignies, C., Norton, T., Beeser, A., Chernoff, J., and Tybulewicz, V.L. (2004). Vav1 transduces T cell receptor signals to the activation of the Ras/ERK pathway via LAT, Sos, and RasGRP1. J Biol Chem *279*, 18239-18246.

236. Narita, T., Weinert, B.T., and Choudhary, C. (2019). Functions and mechanisms of non-histone protein acetylation. Nat Rev Mol Cell Biol *20*, 156-174.

237. Kuhlmann, N., Wroblowski, S., Knyphausen, P., de Boor, S., Brenig, J., Zienert, A.Y., Meyer-Teschendorf, K., Praefcke, G.J., Nolte, H., Kruger, M., *et al.* (2016). Structural and Mechanistic Insights into the Regulation of the Fundamental Rho Regulator RhoGDIalpha by Lysine Acetylation. J Biol Chem *291*, 5484-5499.

238. Kuhlmann, N., Wroblowski, S., Scislowski, L., and Lammers, M. (2016). RhoGDIalpha Acetylation at K127 and K141 Affects Binding toward Nonprenylated RhoA. Biochemistry *55*, 304-312.

239. Saxena, M., Dykes, S.S., Malyarchuk, S., Wang, A.E., Cardelli, J.A., and Pruitt, K. (2015). The sirtuins promote Dishevelled-1 scaffolding of TIAM1, Rac activation and cell migration. Oncogene *34*, 188-198.

240. Ijuin, T., and Takenawa, T. (2012). Regulation of insulin signaling by the phosphatidylinositol 3,4,5-triphosphate phosphatase SKIP through the scaffolding function of Pak1. Mol Cell Biol *32*, 3570-3584.

241. Chiu, T.T., Sun, Y., Koshkina, A., and Klip, A. (2013). Rac-1 superactivation triggers insulin-independent glucose transporter 4 (GLUT4) translocation that bypasses signaling defects exerted by c-Jun N-terminal kinase (JNK)- and ceramide-induced insulin resistance. J Biol Chem *288*, 17520-17531.

242. Sylow, L., Jensen, T.E., Kleinert, M., Hojlund, K., Kiens, B., Wojtaszewski, J., Prats, C., Schjerling, P., and Richter, E.A. (2013). Rac1 signaling is required for insulin-stimulated glucose uptake and is dysregulated in insulin-resistant murine and human skeletal muscle. Diabetes *62*, 1865-1875.

243. Higuchi, M., Onishi, K., Kikuchi, C., and Gotoh, Y. (2008). Scaffolding function of PAK in the PDK1-Akt pathway. Nat Cell Biol *10*, 1356-1364.

244. Hodakoski, C., Hopkins, B.D., Barrows, D., Mense, S.M., Keniry, M., Anderson, K.E., Kern, P.A., Hawkins, P.T., Stephens, L.R., and Parsons, R. (2014). Regulation of PTEN inhibition by the pleckstrin homology domain of P-REX2 during insulin signaling and glucose homeostasis. Proc Natl Acad Sci U S A *111*, 155-160.

245. Luo, J., Sobkiw, C.L., Hirshman, M.F., Logsdon, M.N., Li, T.Q., Goodyear, L.J., and Cantley, L.C. (2006). Loss of class IA PI3K signaling in muscle leads to impaired muscle growth, insulin response, and hyperlipidemia. Cell Metab *3*, 355-366.

246. Kim, J.K., Michael, M.D., Previs, S.F., Peroni, O.D., Mauvais-Jarvis, F., Neschen, S., Kahn, B.B., Kahn, C.R., and Shulman, G.I. (2000). Redistribution of substrates to adipose tissue promotes obesity in mice with selective insulin resistance in muscle. J Clin Invest *105*, 1791-1797.

247. Bruning, J.C., Michael, M.D., Winnay, J.N., Hayashi, T., Horsch, D., Accili, D., Goodyear, L.J., and Kahn, C.R. (1998). A muscle-specific insulin receptor knockout exhibits features of the metabolic syndrome of NIDDM without altering glucose tolerance. Mol Cell *2*, 559-569.

APPENDIX I: PUBLICATIONS

PUBLICATIONS

Other work developed during this period and not described here has led so far to the publication of the following articles.

1. Barreira, M., **Rodriguez-Fdez, S.** and Bustelo, X.R. (2018) New insights into the Vav1 activation cycle in lymphocytes. Cell Signal 45, 132-144.

2. Bustelo, X.R., Crespo, P., Fernandez-Pisonero, I. and **Rodriguez-Fdez, S.** (2018) RAS GTPase–dependent pathways in developmental diseases: old guys, new lads, and current challenges. Curr Opin Cell Biol 55, 42-51.

3. Lorenzo-Martin, L.F., Citterio, C., Menacho-Marquez, M., Conde, J., Larive, R.M., **Rodriguez-Fdez, S.**, Garcia-Escudero, R., Robles-Valero, J., Cuadrado, M., Fernandez-Pisonero, I., Dosil, M., Sevilla, M.A., Montero, M.J., Fernandez-Salguero, P.M., Paramio, J.M. and Bustelo, X.R. (2019) Vav proteins maintain epithelial traits in breast cancer cells using miR-200c-dependent and independent mechanisms. Oncogene 38(2), 209-227.

4. Lorenzo-Martin, L.F., Menacho-Marquez, M., Fabbiano, S., Al-Massadi, O., Abad, A., **Rodriguez-Fdez, S.**, Sevilla, M.A., Montero, M.J., Dieguez, C., Nogueiras, R. and Bustelo, X.R. (2019) Vagal afferents contribute to sympathoexcitation-driven metabolic dysfunctions. J Endocrinol 240(3), 483-496.

5. **Rodríguez-Fdez, S.** and Bustelo, X.R. (2019) The Vav GEF family: an evolutionary and functional perspective. Cells 8, 465.

APPENDIX II: RESUMEN EN CASTELLANO

TÍTULO DE LA TESIS DOCTORAL

CARACTERIZACIÓN DE NUEVOS MECANISMOS DE REGULACIÓN Y FUNCIONES METABÓLICAS DE LAS PROTEÍNAS VAV

ÍNDICE

RESUMEN DE LA INTRODUCCIÓN

1. La familia de proteínas Vav

La función principal de las proteínas de la familia Vav es la de actuar como activadoras de las GTPasas de la familia Rho. Estas GTPasas regulan procesos en las células alternando entre un estado activo (unido a GTP) e inactivo (unido a GDP). El control espacial y temporal de su activación está regulado principalmente por los factores de intercambio nucleotídico o GEFs, entre los que se encuentran las proteínas Vav. Estos factores favorecen el intercambio de GDP por GTP, lo que facilita la rápida activación de las GTPasas.

Las proteínas Vav, ya desde su aparición en coanoflagelados, presentan una estructura en 8 dominios altamente conservada. Esta arquitectura molecular les permite llevar a cabo además de su función catalítica dependiente de los dominios centrales de la molécula (DH-PH-ZF), un gran número de funciones no catalíticas en las que intervienen otros dominios de la proteína.

La regulación de estas proteínas depende principalmente de un mecanismo de inhibición intramolecular regulado a través de fosforilación en tirosinas. En estado inactivo, las proteínas Vav se encuentran en una conformación cerrada en la que los dominios CH, Ac y CSH3 se pliegan sobre la región central DH-PH-ZF. Esto impide tanto su actividad catalítica como gran parte de las adaptadoras. La fosforilación de las proteínas Vav en tirosinas específicas provoca un cambio de conformación que elimina estos contactos intramoleculares, lo que permite su activación. Además de este mecanismo, también afectan a la actividad de las proteínas Vav otros factores entre los que se encuentra la localización subcelular y modificaciones postraduccionales como la metilación en argininas o, potencialmente, la acetilación en lisinas.

En mamíferos existen tres miembros de la familia Vav: Vav1, Vav2 y Vav3. Mientras que la expresión de la primera se restringe al sistema hematopoyético, donde juega un papel especialmente relevante en linfocitos T, las otras dos formas se expresan ubicuamente. Sus funciones son diversas y afectan a diferentes sistemas, incluyendo el sistema hematopoyético, el sistema nerviosos central o el sistema cardiovascular. Además, también son altamente relevantes en diferentes procesos tumorales.

2. Regulación del metabolismo

La regulación del metabolismo requiere la acción coordinada de un gran número de órganos que, a su vez, están regulados por señales nerviosas y endocrinas. Los principales órganos implicados en esta regulación son el sistema nervioso central, el páncreas, el tracto digestivo, el hígado, el tejido adiposo blanco, la grasa parda y el músculo esquelético. El sistema inflamatorio, los glucocorticoides, las catecolaminas y sustancias análogas a hormonas segregadas por los órganos citados contribuyen también al control de la homeostasis metabólica.

La insulina segregada por el páncreas juega un papel primordial en la regulación de los niveles de glucosa a nivel de organismo. Esta hormona actúa sobre los órganos sensibles a través del receptor de insulina, que, a su vez, estimula la ruta de PI3K/Akt. Ello favorece la síntesis proteica, la captación de glucosa, la síntesis de glucógeno y el crecimiento celular. La desregulación de esta ruta de señalización lleva al desarrollo de defectos metabólicos. Una de las dianas principales de esta hormona es el músculo esquelético, que es el responsable de la captación de entre el 60 y el 80% de la glucosa circulante. No es sorprendente, por tanto, que defectos en señalización de insulina en el músculo o alteraciones en la proporción de masa muscular estén asociados al desarrollo de síndrome metabólico y diabetes tipo 2.

3. Masa muscular y proteostasis

El control de la cantidad de masa muscular depende del equilibrio entre la producción y la degradación de proteínas. El regulador principal del crecimiento muscular es el factor de crecimiento IGF-1, el cual señaliza a través de una ruta semejante a la de la insulina. Otros factor importante es la miostatina, que regula negativamente el proceso inhibiendo la diferenciación y la síntesis proteica. Se ha visto que el aumento de la masa muscular mediante alteraciones en cualquiera de estas dos vías en ratones conlleva una mejor sensibilidad a insulina y protección frente a la obesidad inducida por dieta rica en grasa. Un segundo factor importante en la formación de músculo son las células satélite o stem musculares. Especialmente relevantes en músculo en formación o procesos regenerativos, estas células se encargan de formar fibras a través de un proceso de diferenciación denominado miogénesis.

RESUMEN DE LOS RESULTADOS

1. Fosfatidilinositol monofosfatos regulan la activación optima de las rutas efectoras de Vav1

Vav1 es la única proteína de la familia que presenta una región rica en lisinas (KR) entre el dominio ZF y el cassette SH3-SH2-SH3. Esta región está totalmente ausente en Vav2 y en el caso de Vav3 está presente con aminoácidos básicos mucho más dispersos y en menor cantidad. Para analizar su papel en la regulación de Vav1, se realizaron mutantes que alteraban esta región haciéndola más ácida ($KR1^{Mut}$) o más básica ($KR2^{Mut}$). La actividad de estas formas mutadas se testó en linfocitos T mediante ensayos de actividad luciferasa, hallando que la versión $KR1^{Mut}$ inducía una menor activación de NFAT y JNK que la forma WT de Vav1. La forma $KR2^{Mut}$, por su parte, provocaba una hiperactivación de ambos factores de transcripción. El uso de estos mutantes nos permitió comprobar también que esta región contribuye a las funciones mediadas por Vav1 en linfocitos T pero no así en otras líneas celulares. Además, utilizando formas truncadas e hiperactivas de Vav1, pudimos demostrar que esta regulación es independiente del sistema de inhibición intramolecular mediado por fosforilación característico de esta familia de proteínas. El uso de mutantes puntuales en los que los aminoácidos más ácidos de esta zona fueron sustituidos por lisinas demostró que esta modulación de la actividad catalítica y adaptadora de Vav1 está parcialmente relacionada con las propiedades electrostáticas de esta región.

Ensayos de fluorescencia y de fraccionamiento subcelular mostraron que alteraciones en la región KR afectan a la localización de Vav1 en la membrana plasmática. Además, la localización de Vav1 durante la sinapsis inmunológica y la polimerización de actina también se ven afectadas al mutar la región rica en lisinas. Para demostrar que la baja actividad del mutante KR1 era debida a problemas en la localización de esta proteína, se añadió la secuencia CAAX de H-Ras en el extremo C-terminal de la proteína para forzar su anclaje a la membrana plasmática. Apoyando nuestra hipótesis, esta modificación rescataba tanto la actividad catalítica como la activación de NFAT mediada por Vav1 en linfocitos T.

Los datos anteriores sugerían que la región KR podría estar implicada en un proceso de interacción con fosfolípidos en la membrana plasmática. Para testar esta

hipótesis, se realizaron diferentes experimentos de unión a lípidos utilizando diferentes formas mutantes de la proteína Vav1 fusionadas a MBP. Estas proteínas fueron purificadas de bacterias y su capacidad de unión a lípidos ensayada tanto en filtro lipídico como a través del uso de liposomas. Nuestros experimentos demostraron que Vav1 es capaz de interaccionar con alta afinidad con PI5P, PI3P y PI4P pero no con otros fosfolípidos de membrana. Además, las formas mutantes $KR1^{Mut}$ o $KR2^{Mut}$ presentan menor y mayor afinidad por estos lípidos, respectivamente. Ensayos posteriores demostraron que esta capacidad de unión a lípidos reside en la región KR pero requieren un dominio bipartito compuesto por el ZF y la región polibásica adyacente de Vav1.

Por último, para demostrar que el lípido PI5P juega un papel en la señalización de Vav1, nos valimos de la enzima bacteriana IpgD, una $PI(4,5)P_2$ fosfatasa, para incrementar artificialmente la cantidad de PI5P en linfocitos T. Los resultados mostraron que el incremento en la proporción de este lípido en la célula favorecía la actividad catalítica de Vav1.

2. La acetilación en lisinas de Vav1 regula negativamente la activación de NFAT

Diferentes estudios de espectrometría de masas han detectado acetilación en lisinas en los tres miembros de la familia Vav. Esta modificación posttraduccional, que se creía exclusiva de histonas, ha ganado interés en los últimos años al comprobar su alta prevalencia en proteínas tanto nucleares como citoplasmáticas.

Con el fin de determinar si la acetilación podría tener relevancia *in vivo* en la regulación de Vav1, se estudiaron tanto las dinámicas generales de activación como el efecto individual de las lisinas identificadas mediante espectrometría de masas.

Para abordar el primer punto, se realizaron experimentos inmunoprecipitando Vav1 y detectando la fracción acetilada mediante un anticuerpo específico contra lisinas acetiladas. Pudimos comprobar de esta forma que Vav1 se acetila en respuesta a estímulos mitogénicos, como pueden ser la estimulación con EGF en fibroblastos o con anti-CD3 en linfocitos T, de forma similar a lo que ocurre con la fosforilación. La mutación G691V, inactivante del dominio SH2 de interacción con proteínas fosforiladas, impedía tanto la acetilación como la fosforilación de la proteína. Sin embargo, ensayos de fraccionamiento celular demostraron que esta modificación se encuentra restringida al compartimento citoplasmático.

Con el fin de identificar las consecuencias de esta modificación, se seleccionaron aquellos residuos a priori más interesantes debido bien a su identificación en varios ensayos o bien a la relevancia de su localización en base a estudios anteriores. Estos residuos fueron mutados a arginina o a glutamina para imitar la forma no acetilable o constitutivamente acetilada, respectivamente. Comprobamos que la mayoría de estas mutaciones no afectaban a la actividad catalítica de la proteína y, en el caso de las que sí lo hacían, la mutación a arginina y a glutamina tenía el mismo efecto. Estos datos indican que la acetilación de Vav1 no afecta a su actividad catalítica. No ocurre lo mismo con la actividad no catalítica. La mutación de estas lisinas a arginina y glutamina mostró efectos diferenciales en la capacidad de Vav1 para activar NFAT. En concreto, las lisinas K^{194}, K^{222}, K^{252}, K^{587} y K^{716} mutadas a la forma "acetilada" mostraban una reducción de la actividad de NFAT, mientras que en la versión no acetilable la actividad no se veía alterada o incluso se incrementaba. Además, la mutación conjunta de las lisinas K^{222}, K^{252} y K^{716} resultaba en la total inactivación de esta vía. Análisis más exhaustivos nos

permitieron comprobar que no todos los mutantes menos activos seguían un mismo mecanismo regulatorio.

Además, a pesar de que los residuos equivalentes a la lisina K^{716} en Vav2 y Vav3 también se han identificado como acetilados en estudios masivos de espectrometría de masas, la mutación de los mismos no resulta en la pérdida de fosforilación en estado basal ni en reducciones tan marcadas de la capacidad para activar NFAT como las observadas para Vav1. Estos resultados indican que este mecanismo regulatorio es específico no solo de tipo celular sino también de este miembro de la familia en concreto.

3. Rutas dependientes de la actividad catalítica de Vav2 contribuyen al crecimiento del músculo esquelético y la homeostasis metabólica.

En este estudio, se utilizaron ratones modificados genéticamente para indagar en nuevos procesos fisiológicos regulados por Vav2 que sean dependientes de su actividad catalítica. Para ello, se generaron dos modelos de ratón *knock-in* opuestos. En el primer modelo, la forma silvestre fui sustituída por una versión que presenta una mutación puntual que reduce sustancialmente la actividad catalítica de Vav2 ($Vav2^{L332A/L332A}$). En el segundo modelo, la forma silvestre fue sustituída por una forma truncada que se encuentra constitutivamente activa debido a la pérdida del mecanismo de regulación intramolecular dependiente de fosforilación ($Vav2^{Onc/Onc}$). En ambos casos la forma alterada está bajo el control del promotor endógeno de Vav2.

Los análisis de estos ratones mostraron que los ratones $Vav2^{L332A/L332A}$ tienen menor masa magra que sus correspondientes WT, mientras que los ratones $Vav2^{Onc/Onc}$ presentan el fenotipo opuesto. Además, los primeros tienden a acumular mayor cantidad de grasa que sus controles con el paso del tiempo, lo contrario que ocurre con los segundos. El estudio del tamaño de los músculos de la pata trasera de los ratones a diferentes edades confirmó que la actividad catalítica de Vav2 afecta la cantidad de masa muscular. Además, estas diferencias se relacionan con menor (en el caso de ratones $Vav2^{L332A/L332A}$) o mayor (en ratones $Vav2^{Onc/Onc}$) tamaño de las fibras musculares. Se comprobó también que las células satélite o madre musculares provenientes de ratones $Vav2^{L332A/L332A}$ y $Vav2^{Onc/Onc}$ proliferaban respectivamente menos y más que las provenientes de sus controles WT.

Mediante ensayos de inyección de insulina o IGF-1 a través de la vena cava pudimos demostrar que la respuesta del músculo a estos factores se encontraba disminuida en el caso de los ratones Vav2 catalíticamente deficientes e incrementada en los constitutivamente activos. En otros órganos no se encontró ningún tipo de alteración a excepción de un incremento de la sensibilidad a insulina en el tejido adiposo de los ratones $Vav2^{Onc/Onc}$. Estos datos se confirmaron utilizando una línea celular de mioblastos. Además, demostramos que Vav2 es importante para la activación óptima de la ruta PI3K-Akt.

A continuación, se profundizó en las consecuencias metabólicas de la alteración de la actividad catalítica de Vav2. Comprobamos que la tolerancia a glucosa de los

ratones *Vav2*$^{L332A/L332A}$ se encuentra disminuida tanto en condiciones de dieta normal como en condiciones de dieta rica en grasa. Además, la respuesta sistémica a insulina también se encontraba alterada en ambos casos. Los ratones padecían hiperglicemia a partir de los 8 meses de edad. Por el contrario, ratones *Vav2*$^{Onc/Onc}$ mostraban una mejor tolerancia a glucosa y mejor respuesta a la infusión de insulina en ambos tipos de dieta. La secreción de insulina era normal en ambos modelos murinos.

En consonancia con los datos anteriores, el peso de los ratones *Vav2*$^{L332A/L332A}$ mantenidos con dieta grasa aumenta más y más rápidamente que el de sus correspondientes controles. La cantidad de grasa abdominal y el tamaño de los adipocitos en estos animales también fue mayor tanto con dieta grasa como con dieta normal. Además, su gasto energético y su cociente respiratorio durante la fase diurna eran menores que los de los animales WT. Los ratones *Vav2*$^{L332A/L332A}$ también presentaban mayor cantidad de triglicéridos en hígado y una ligera esteatosis a los 6 meses de edad. Esta mayor acumulación de lípidos en hígado era más evidente en ratones sometidos a dieta rica en grasa. Por el contrario, los ratones *Vav2*$^{Onc/Onc}$ estaban protegidos frente a la obesidad inducida por dieta rica en grasa y mostraban adipocitos de menor tamaño tanto en dieta control como en dieta rica en grasa. Su gasto energético y su cociente respiratorio durante el día eran mayores que los de sus homólogos WT. Sin embargo, no se encontró ninguna diferencia significativa en hígado.

En la grasa parda también se observaron fenotipos opuestos en los dos modelos animales empleados. Los ratones *Vav2*$^{L332A/L332A}$ presentaban un menor número de adipocitos por campo a partir de los 4 meses de edad y gotas lipídicas de mayor tamaño ya desde los 2.5 meses. Además, encontramos que la expresión de la proteína desacoplante Ucp1, necesaria para la termogénesis, y la lipasa Hsl era menor que en los controles. La administración de dieta rica en grasa empeora el fenotipo observado en los ratones *Vav2*$^{L332A/L332A}$. De forma contraria, el número de adipocitos marrones y la expresión de Ucp1 y Hsl era mayor en los animales *Vav2*$^{Onc/Onc}$ de 4 meses que en sus controles y el tamaño de las gotas lipídicas menor. Estas diferencias eran mucho más evidentes en animales alimentados con dieta rica en grasa.

Por último, el análisis ordenado de todos los defectos nos permitió comprobar que las alteraciones en músculo eran las primeras en ser observadas, apoyando la hipótesis de que las alteraciones en la señalización de IGF-1 e insulina en este órgano son las causantes de todo el fenotipo metabólico observado.

CONCLUSIONES

1. La interacción de Vav1 con fosfatidilinositol monofosfatos contribuye a su señalización en linfocitos T. Esta capa de regulación, dependiente de la región rica en lisinas en cooperación con el dominio ZF, es específica para este miembro de la familia Vav y para este tipo celular.

2. La acetilación de Vav1 en residuos de lisina específicos reduce la estimulación de la ruta de NFAT. La fracción de Vav1 acetilado aumenta tras estimulación del TCR y se encuentra en el compartimento citoplasmático.

3. Vav2 promueve la activación óptima de la ruta de PI3K–Akt corriente abajo de IGF–1 e insulina en músculo esquelético.

4. La inhibición sostenida de la actividad GEF de Vav2 conlleva una reducción en la masa muscular y el desarrollo a largo plazo de síntomas similares a síndrome metabólico que se ven agravados tras la administración de dieta rica en grasa. Por el contrario, la hiperactivación crónica de las rutas dependientes de la actividad catalítica de Vav2 produce hipertrofia muscular y protección frente a la obesidad inducida por dieta y comorbilidades asociadas a ésta.